J. Fluid Mech. (2006), *vol.* 561, *pp.* 147–180.
doi:10.1017/S0022112006000310 Printed in the United Kingdom

Defining the 'modified Griffin plot' in vortex-induced vibration: revealing the effect of Reynolds number using controlled damping

By R. N. GOVARDHAN[1] AND C. H. K. WILLIAMSON[2]

[1]Department of Mechanical Engineering, Indian Institute of Science, Bangalore – 560012, India

[2]Sibley School of Mechanical and Aerospace Engineering, Cornell University, Ithaca, NY 14853-7501, USA

(Received 21 February 2005 and in revised form 10 January 2006)

In the present work, we study the transverse vortex-induced vibrations of an elastically mounted rigid cylinder in a fluid flow. We employ a technique to accurately control the structural damping, enabling the system to take on both negative and positive damping. This permits a systematic study of the effects of system mass and damping on the peak vibration response. Previous experiments over the last 30 years indicate a large scatter in peak-amplitude data (A^*) versus the product of mass–damping (α), in the so-called 'Griffin plot'.

A principal result in the present work is the discovery that the data collapse very well if one takes into account the effect of Reynolds number (Re), as an extra parameter in a modified Griffin plot. Peak amplitudes corresponding to zero damping ($A^*_{\alpha=0}$), for a compilation of experiments over a wide range of $Re = 500$–$33\,000$, are very well represented by the functional form $A^*_{\alpha=0} = f(Re) = \log(0.41\,Re^{0.36})$. For a given Re, the amplitude A^* appears to be proportional to a function of mass–damping, $A^* \propto g(\alpha)$, which is a similar function over all Re. A good best-fit for a wide range of mass–damping and Reynolds number is thus given by the following simple expression, where $A^* = g(\alpha)\,f(Re)$:

$$A^* = (1 - 1.12\,\alpha + 0.30\,\alpha^2)\,\log(0.41\,Re^{0.36}).$$

In essence, by using a renormalized parameter, which we define as the 'modified amplitude', $A^*_M = A^*/A^*_{\alpha=0}$, the previously scattered data collapse very well onto a single curve, $g(\alpha)$, on what we refer to as the 'modified Griffin plot'. There has also been much debate over the last three decades concerning the validity of using the product of mass and damping (such as α) in these problems. Our results indicate that the combined mass–damping parameter (α) does indeed collapse peak-amplitude data well, at a given Re, independent of the precise mass and damping values, for mass ratios down to $m^* = 1$.

1. Introduction and preliminary work

The problem of vortex-induced vibration of structures is important in many fields of engineering. For example, it is a cause for concern in the dynamics of riser tubes bringing oil from the seabed to the surface, in flow around heat exchanger tubes, in the dynamics of civil engineering structures such as bridges and chimneys, and also in many other situations of practical importance. This has led to a large number of

fundamental studies that are summarized in the comprehensive reviews of Sarpkaya (1979), Griffin & Ramberg (1982), Bearman (1984), Parkinson (1989), Williamson & Govardhan (2004) and in the books by Blevins (1990), Naudascher & Rockwell (1994), Sumer & Fredsoe (1997); and in Anagnostopoulos (2002). In spite of this large number of studies, several fundamental questions remain unanswered even in the simple case of the elastically mounted cylinder, as discussed in the recent review of Williamson & Govardhan (2004). One of the most important of these unanswered questions is the relationship between the maximum cylinder response amplitude and the system mass and damping.

Generally in the literature, the peak response amplitude has been plotted versus the 'Skop–Griffin' parameter, which is proportional to the product of mass and damping, following the first comprehensive compilation of existing data by Griffin and coworkers in the 1970s (e.g. Griffin, Skop & Ramberg 1975), and labelled for convenience the 'Griffin plot' by Khalak & Williamson (1999). Surprisingly, even the very basic fact of whether a combined mass–damping parameter could reasonably collapse peak-amplitude data has been debated for almost three decades (see Sarpkaya 1978, 1979, 1995, for example). In fact, owing to the scatter and trend of data in the 'Griffin plot', Williamson & Govardhan (2004), in their review paper, stated: 'One can conclude that, despite the enormous effort over the last 25 years to critique and define accurately this useful plot, it is not yet fully defined'. It is the new definition of this plot, for an elastically mounted rigid cylinder, that is at the heart of the present contribution.

Typically in previous studies, given the lack of direct control on structural damping, the maximum amplitude information has been compiled from a number of quite different experimental arrangements, leading to substantial uncertainties. In the present study, we circumvent this problem by employing an external active damper, which is capable of implementing controlled negative and positive damping on the oscillating system. Recall that the first classical experiments where positive damping was controlled (at high values of mass–damping) were conducted by Feng (1968), using the eddy–current approach. Other recent experimental studies, where damping has been directly controlled, are the force-feedback system of Hover, Miller & Triantafyllou (1997), and the recent experiments of Klamo, Leonard & Roshko (2004, 2005). The lowest mass–damping parameter (see table 1) achieved in Klamo *et al.* (2005) was around 0.007. In the case of Hover *et al.* (1997), although in principle one can specify zero damping in the virtual cable testing apparatus, in practice an effective minimum mass–damping value of about 0.013 is achievable, as discussed in Hover, Techet & Triantafyllou (1998).

In the present case, the design of our damper system allows us to vary the damping from negative values, inducing large-amplitude response, to high damping, where vibration becomes negligible. Using damping control, we seek in this study to understand the following fundamental unanswered questions regarding the 'Griffin plot', recently outlined in the review of Williamson & Govardhan (2004):

(i) Under what conditions does the classically employed mass–damping parameter collapse peak-amplitude data?

(ii) What is the maximum possible amplitude attainable for a cylinder undergoing vortex-induced vibration (VIV), for conditions of extremely small mass and damping?

(iii) What is the functional shape for a plot of peak amplitude versus mass–damping? In fact, one might ask: Is there indeed a unique functional shape? We shall show in the present work that there is no unique function relating peak amplitude to mass–damping, because of the effect of Reynolds number on response amplitude.

Mass ratio	m^*	$\dfrac{m}{\pi\rho D^2 L/4}$
Damping ratio	ζ	$\dfrac{c}{2\sqrt{k(m+m_A)}}$
Mass–damping parameter	α	$(m^*+C_A)\zeta$
Velocity ratio	U^*	$\dfrac{U}{f_N D}$
Amplitude ratio	A^*	$\dfrac{A}{D}$
Frequency ratio	f^*	$\dfrac{f}{f_N}$
Transverse force coefficient	C_Y	$\dfrac{F}{\frac{1}{2}\rho U^2 DL}$
Reynolds number	Re	$\dfrac{\rho U D}{\mu}$

TABLE 1. Non-dimensional groups for the elastically mounted cylinder. The frequency ratio f^* is defined as (f/f_N), where f is the oscillation frequency, and f_N is the natural frequency in water. The ideal added mass, m_A, is given by $m_A = C_A m_d$, where m_d is the displaced fluid mass and C_A is the potential added mass coefficient. ($C_A = 1.0$ for a circular cylinder). D = cylinder diameter, L = cylinder length, ρ = fluid density, U = free-stream velocity, μ = viscosity.

However, despite this dependence of response amplitude on the Reynolds number, we shall show that it is possible to introduce a 'modified amplitude' that is independent of Reynolds number, and obtain a unique functional relationship for this 'modified amplitude' with mass–damping.

Before addressing the above questions, we shall briefly introduce an equation of motion generally used to represent the vortex-induced vibrations of a cylinder in the transverse y-direction (perpendicular to the free stream), as follows:

$$m\ddot{y} + c\dot{y} + ky = F, \tag{1.1}$$

where m = total oscillating structural mass (i.e. not including added mass); c = structural damping; k = spring constant; F = fluid force in the transverse direction. When the body oscillation frequency is synchronized with the periodic vortex wake mode, reasonable approximations to the force, $F(t)$, and the response displacement $y(t)$, are often given as

$$F(t) = F_o \sin(\omega t + \phi), \tag{1.2}$$

$$y(t) = A \sin(\omega t), \tag{1.3}$$

where $\omega = 2\pi f$; f = oscillation frequency. The phase angle ϕ, between the fluid force and the body displacement, is crucial in determining the energy transfer from the fluid motion to the body motion, and hence in influencing the amplitude of oscillation, as pointed out clearly in several review papers (e.g. Bearman 1984). We select a set of relevant non-dimensional parameters in this problem, which are presented in table 1.

The response amplitude and frequency may be derived in a straightforward manner from equations (1.1)–(1.3), and are formulated here, along the lines of Khalak &

Williamson (1999), as follows:

$$A^* = \frac{1}{4\pi^3}\frac{C_Y \sin\phi}{(m^* + C_A)\zeta}\left(\frac{U^*}{f^*}\right)^2 f^*, \tag{1.4}$$

$$f^* = \sqrt{\frac{(m^* + C_A)}{(m^* + C_{EA})}}, \tag{1.5}$$

where C_A is the potential flow added mass coefficient ($C_A = 1.0$ for a circular cylinder), and C_{EA} is an 'effective' added mass coefficient that includes an apparent effect due to the total transverse fluid force in phase with the body acceleration ($C_Y \cos\phi$):

$$C_{EA} = \frac{1}{2\pi^3 A^*}\left(\frac{U^*}{f^*}\right)^2 C_Y \cos\phi, \tag{1.6}$$

where these non-dimensional groups $\{A^*, U^*, f^*, C_Y, m^*\}$ are defined in table 1.

A significant question that has been debated for many years is whether a combined mass–damping parameter [$m^*\zeta$ or $(m^* + C_A)\zeta$] could reasonably collapse peak-amplitude data A^*_{max} in the Griffin plot. (By the terminology 'peak amplitude', we mean the maximum amplitude found over a complete response plot, as flow velocity is varied. See for example the bull's eye symbols in figure 3.) The use of a mass–damping parameter stems from several studies (see for example, Vickery & Watkins 1964; Scruton 1965). Skop & Griffin (1973) compiled data from several different investigators as a means to usefully predict response amplitudes. Their combined response parameter was subsequently termed S_G in Skop (1974), and was termed the Skop–Griffin parameter in Khalak & Williamson (1999) (which is, in fact, the origin of the initials S and G):

$$\text{Skop–Griffin parameter} = S_G = 2\pi^3 S^2 (m^*\zeta), \tag{1.7}$$

where S is the Strouhal number of the static cylinder. The logic in choosing a combined mass–damping parameter comes from equation (1.4) for A^*. For example, Bearman (1984) demonstrated that for large mass ratios ($m^* \gg 1$), the actual cylinder oscillation frequency (f) at resonance will be close to the vortex shedding frequency for the static cylinder (f_V), and also close to the system natural frequency (f_N), i.e. $f \approx f_V \approx f_N$, and thus $f^* \approx 1.0$ (see equation (1.5) for large m^*). Thus, at resonance, the parameter $(U^*/f^*) = (U/fD) \approx (U/f_V D) = 1/S$, where S is the Strouhal number of the static cylinder, suggesting a resonance at the normalized velocity, $U^* \approx 5-6$. Therefore, the assumption is often made that both (U^*/f^*) and f^* are constants, under resonance conditions, giving (from equation (1.4))

$$A^*_{max} \propto \frac{C_Y \sin\phi}{(m^* + C_A)\zeta}. \tag{1.8}$$

If (U^*/f^*) is assumed constant, then the excitation ($C_Y \sin\phi$) is a function of A^* only. Therefore, under these assumptions, A^*_{max} is a function only of the product of mass and damping $(m^* + C_A)\zeta$, henceforth referred to by the symbol α (see table 1). However, it is not self-evident that $f^* \sim 1$. Repeated concerns over the use of such a combined mass–damping parameter at low mass ratios have been clearly discussed by Sarpkaya (see for example Sarpkaya 1978, 1979, 1995 and several other papers) and by Zdravkovich (1990). However, the experiments of Griffin & Ramberg (1982) and the more recent results of Khalak & Williamson (1999), suggest that the use of a single combined mass–damping parameter (α) does collapse peak-amplitude data

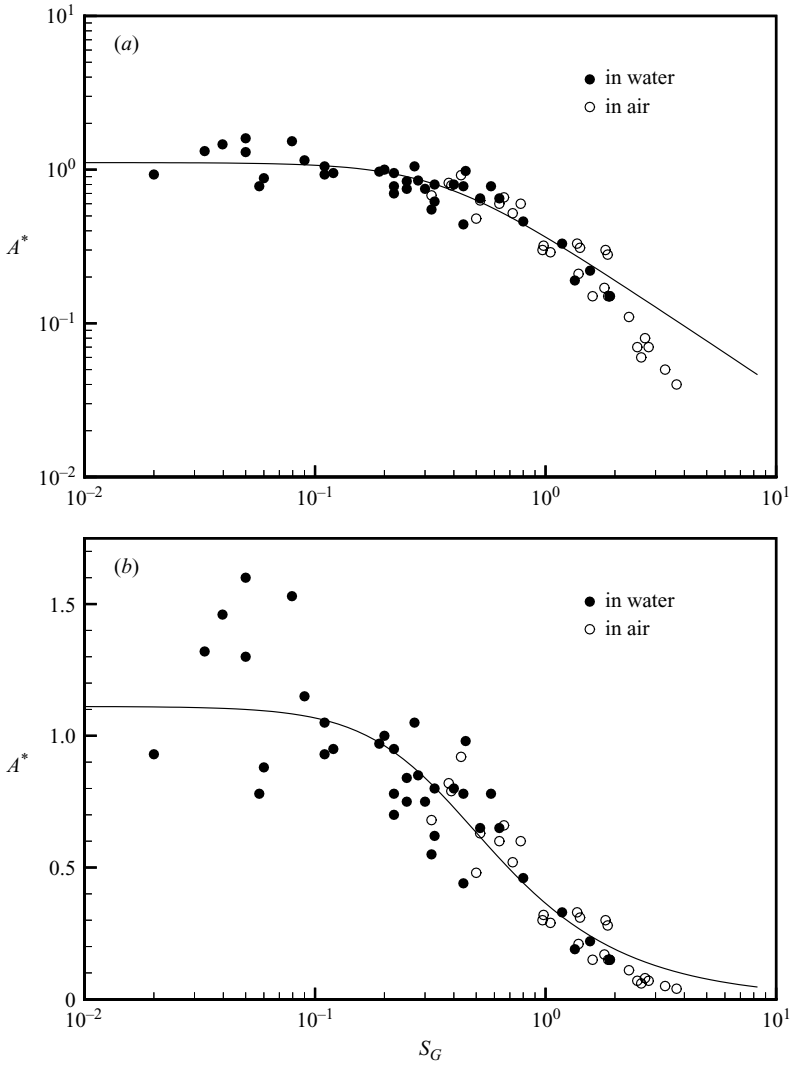

FIGURE 1. The 'Griffin' plot. (*a*) The classical Griffin plot using peak-amplitude data (A^*) on a logarithmic axis versus the Skop–Griffin parameter (S_G), as collected and plotted by Skop & Balasubramanian (1997). In (*b*), the large scatter in the data in (*a*) is revealed when one uses a linear axis for the amplitude.

quite well, under limited conditions. We shall directly address this issue in the present work, by obtaining peak response amplitudes for a set of mass ratios, while keeping the mass–damping parameter fixed. These experiments are made possible by our techniques to control damping.

Griffin *et al.* (1975) compiled the first extensive set of peak-amplitude data from many different investigations, using the combined mass–damping parameter (S_G). The classical log-log form of the plot (Griffin 1980), of the type in figure 1(*a*), has become the widely used presentation of peak response data. From this point forward in the paper, we shall use A^* to refer to peak amplitude (in place of A^*_{max}). If we plot an extension of the Griffin plot that was compiled by Skop & Balasubramanian (1997) for a variety of experiments, as in figure 1(*a*), and then modify the plot using a linear

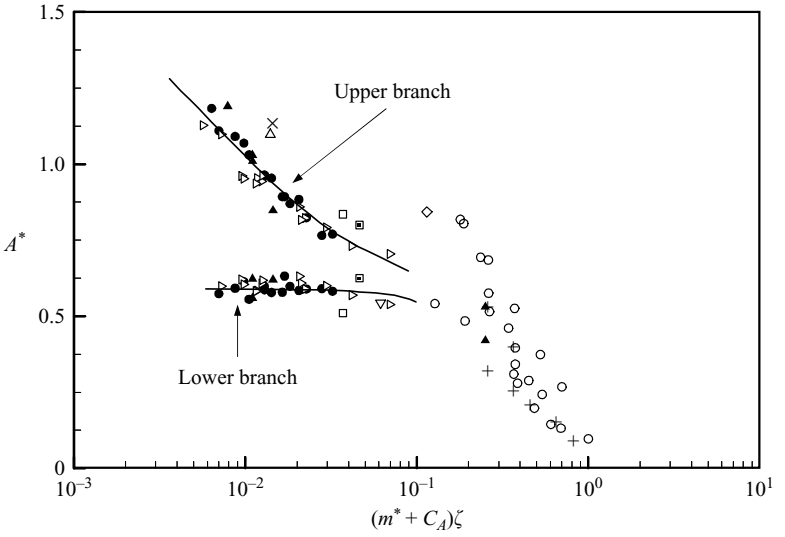

FIGURE 2. An updated Griffin plot using only data for elastically mounted cylinders, restricted to motion transverse to the fluid flow, taken from Williamson & Govardhan (2004). By removing data for quite different VIV systems from figure 1, one can see an approximate trend in the data, but apparently it is not saturating as mass–damping becomes small. ●, Khalak & Williamson (1999); ▲, Govardhan & Williamson (2000); ⊡, Hover *et al.* (1998); ○, Griffin (1980); ▷, Jauvtis & Williamson (2003); △, Moe & Overvik (1982); ▽, Angrilli *et al.* (1972); □, Owen *et al.* (2001); ◇, Gharib *et al.* (1998); +, Feng (1968); ×, Vikestad (1998); ⊕, Anand & Torum (1985).

Y-axis in figure 1(b), we now see significant scatter, not evident by the classical log-log format. The maximum attainable amplitude lies anywhere in the range $A^* = 0.8 - 1.6$. Given this scatter, it does not appear reasonable to collapse data for different VIV systems like the free cylinder, cantilever and pivoted cylinders, in the same plot. In figure 2, we present only those data corresponding to elastically mounted cylinders. Following Khalak & Williamson (1999), we introduce two distinct curves into the Griffin plot, representing the peak amplitudes for both the upper and the lower response branches. (These branches are described below, with reference to figure 3.) The resulting data from these diverse experimental arrangements appear to give an approximate functional relationship between A^*_{max} and mass–damping (α) over a wide range of parameters, applicable for the regime $m^* > 2$, and for $\alpha > 0.006$.

Finally one might observe in figure 2 that, even for the smallest mass–damping, the peak amplitudes are not yet close to some limiting amplitude; the saturation limit has not been reached. Therefore, the Griffin plot has not been fully defined, and the plot in figure 2 is insufficient to deduce the maximum vibration amplitude as mass–damping becomes zero.

Regarding the character of vibration response, the amplitude plot as a function of flow speed for such an elastically mounted cylinder shows two distinctly different types of behaviour, depending on whether one has a high or low combined mass–damping parameter (α), as shown in Khalak & Williamson (1999). In the classical high-α case like in Feng (1968), 'Initial' and 'Lower' amplitude branches are separated by a discontinuous mode transition, as shown in figure 3(a). However, in the case of low-α, a further higher amplitude 'Upper' branch of response appears, and there exist three response branches. There are therefore two mode transitions in this case. The existence of, not one, but two mode transitions at low-α, and their relationship with the forces

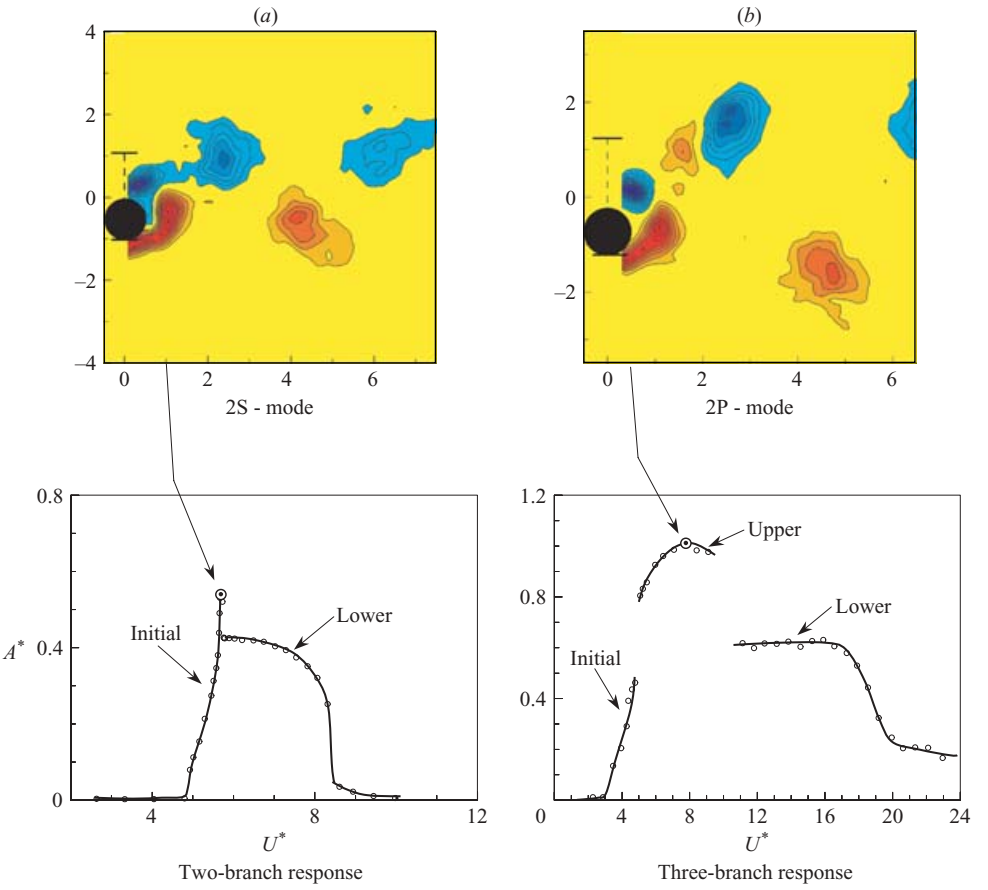

FIGURE 3. Typical two-branch and three-branch response plots. (*a*) The high mass–damping type of response showing only two branches, namely the Initial and Lower branches. At peak response (shown by ⊙), we have the 2S vortex formation mode. (*b*) The low mass–damping type of response showing three branches, namely the Initial, Upper and Lower branches. At peak response we have the 2P vortex formation mode. In this plot, A^* refers to normalized amplitude. The mass–damping parameters are (*a*) $\alpha = 0.256$, (*b*) $\alpha = 0.011$, and the Reynolds numbers for the vorticity fields shown are (*a*) $Re \approx 1250$, (*b*) $Re \approx 3100$. (Govardhan & Williamson 2000).

and wake vortex dynamics, is studied in detail by simultaneous force, displacement and vorticity measurements for a freely vibrating cylinder in Govardhan & Williamson (2000). Of interest in the present work, is the mode of vortex shedding at peak amplitude. As seen from the digital particle image velocimetry (DPIV) vorticity fields shown in figures 3(*a*) and 3(*b*), the vortex formation mode is '2S' for the high-α case, and '2P' in the low-α case; '2S' indicating 2 Single vortices formed per cycle, and '2P' meaning 2 Pairs of counter-rotating vortices formed per cycle, as defined by Williamson & Roshko (1988) based on their forced oscillation experiments. In the case of low α, the second vortex of each vortex pair is weaker than the first, and rapidly decays downstream as seen in figure 3(*b*). (A clearer view of the 2P mode is found for the lower branch response, as shown in Govardhan & Williamson (2000).)

We began this study of the effect of damping on cylinder response in 1998 (we refer to this unpublished study as GW98) after carefully designing an electromagnetic damper capable of providing additional negative or positive damping. Brief details

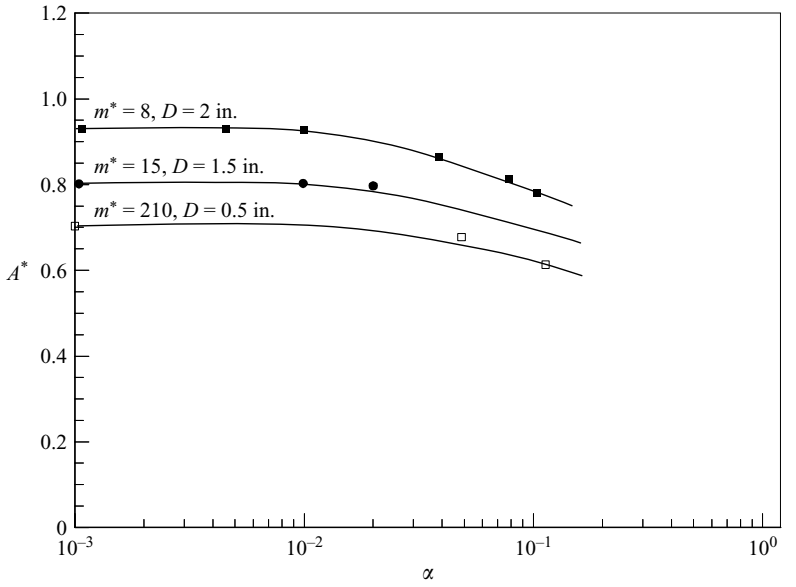

FIGURE 4. Original controlled damping experiments using the electromagnetic damper (GW98). In these early experiments, we interpreted the results as indicating a clear increase in A^* due to a decreasing mass ratio (m^*) even when mass–damping is kept constant (α = constant). However, note that to achieve lower m^* we increase diameter, and thereby also Reynolds number. Therefore, the increase in A^* could also be related to the increase in Re. ■, $m^* = 8$, $D = 2$ in., $Re = 4500$; ●, $m^* = 15$, $D = 1.5$ in., $Re = 2500$; □, $m^* = 210$, $D = 0.5$ in., $Re = 1000$.

of this damper are given in the experimental methods section. After initial checks using 'pluck' tests in air to verify that the system was indeed providing good damping control, the test cylinders were installed and the system was used to obtain peak amplitude data as the damping was varied, at fixed mass ratio. A few different mass ratios were investigated using cylinders of different diameters. The resulting data are shown in figure 4. At this point, the data seemed to suggest that there was an apparent independent effect of mass ratio on the peak amplitudes, even if the combined mass–damping parameter (α) was kept constant. This result seemed rather puzzling, as it was contrary to observations from earlier work of Khalak & Williamson (1997).

After the new results in 1998 were obtained with the (as yet unproven) electro-magnetic damper, we spent some time attempting to understand the apparent contradictions with our earlier work, ultimately diverting our energies to other aspects of VIV. Upon later comparison with the amplitude response data of Hover *et al.* (1998), measured from an ingenious virtual cable testing apparatus, it occurred to us that a basic factor influencing our new results for peak amplitude could possibly be the Reynolds number. In hindsight, the electro-magnetic damper had in fact performed remarkably well. It was leading us to the important deduction that it was not the mass ratio that was influencing our earlier results, but instead it was the fact that, as mass ratio is reduced (by increasing body diameter), the Reynolds number is increased. An increase in peak-amplitude response, as Reynolds number is increased, was subsequently deduced to be a consistent trend with all of our results with the electro-magnetic damper, fitting in very well with all the results of Khalak & Williamson (1999) and Govardhan & Williamson (2000), and much other unpublished

data from our studies. In fact, this trend explains why the data in the Griffin plot of figure 2 apparently were not saturating to a particular amplitude as mass–damping became very small. These deductions naturally led us in 2000–2001 to return to the problem, and to design a rather simpler, and quite different, negative–positive mechanical damper, and it afforded us the possibility also of direct comparison with the original 1998 electro-magnetic damping system. The design of the damper, the comparison to our previous controlled-damping response results, and the ensuing contribution to understanding the Griffin plot, forms the basis of the present paper.

Some preliminary aspects of our present work have been presented in Govardhan & Williamson (2005), where the effect of Reynolds number on vibration and peak amplitude response have been briefly discussed. Our deduction that Reynolds number is a key parameter of peak-amplitude response is consistent with the recent work of the group at MIT under Michael Triantafyllou and Franz Hover. From their controlled vibration experiments, they have found that the regime of positive excitation reaches higher amplitudes if the Reynolds number is increased, as evident from the work at MIT of Smogeli (2002) and subsequently Triantafyllou, Hover & Techet (2004), which would suggest that higher amplitudes would be reached in a VIV system at higher Reynolds numbers. It is important to acknowledge here the recent results of Klamo *et al.* (2005) at Caltech, who have independently set up an eddy-current damping arrangement, with a vertical cylinder on air bearings similar to our own setup at Cornell (Khalak & Williamson 1996). They have found a clear increase in peak amplitude as Reynolds number is increased from $Re = 525$ to 2600. Employing also the compiled data from the review of Williamson & Govardhan (2004), they indicate the general trend of peak amplitudes increasing with Reynolds number, and were the first to make a presentation on this point (Klamo *et al.* 2004). They state in their subsequent paper (Klamo *et al.* 2005) that 'the Reynolds number, which has generally been ignored in discussions of maximum-amplitude data, is an important parameter.' This statement is in direct accordance with our results here.

Following a description of the experimental details in the next section (§ 2), we shall study the effect of mass ratio on the peak amplitude, keeping fixed values of mass–damping and Reynolds number, in § 3. In § 4, we show the effect of positive and negative damping on the character of the amplitude response plot. We then highlight the importance of Reynolds number in determining the peak amplitude, which we study in detail in § 5. We obtain best-fit equations for the functional shape of the Griffin plot in § 6. Finally, in § 7, we show that the large scatter in the conventional Griffin plot is principally due to the effect of *Re*. Using a 'modified amplitude', to take into account this *Re* effect, the scattered data collapse very well onto a single curve in the new 'modified' Griffin plot. This is followed by the conclusions in § 8.

2. Experimental details

The present experiments were conducted using a hydroelastic facility, which is described in detail in Khalak & Williamson (1996, 1999), in conjunction with the Cornell–ONR Water Channel. The hydroelastic facility comprises air bearings mounted above the channel test section, which allow a vertical cylinder in the fluid to move transverse to the free stream. The turbulence level in the test section of the water channel was less than 0.9 %, in the 15 in. × 20 in. (0.381 m × 0.508 m) cross-section, over a range of free-stream velocities, $U = 0.04 - 0.32\,\mathrm{m\,s^{-1}}$. Cylinders of diameters, $D = 0.0191$–0.0508 m, were used in this study with length–diameter ratios, $L/D = 6$–22. In all the experiments, end plates were fixed to the test section and

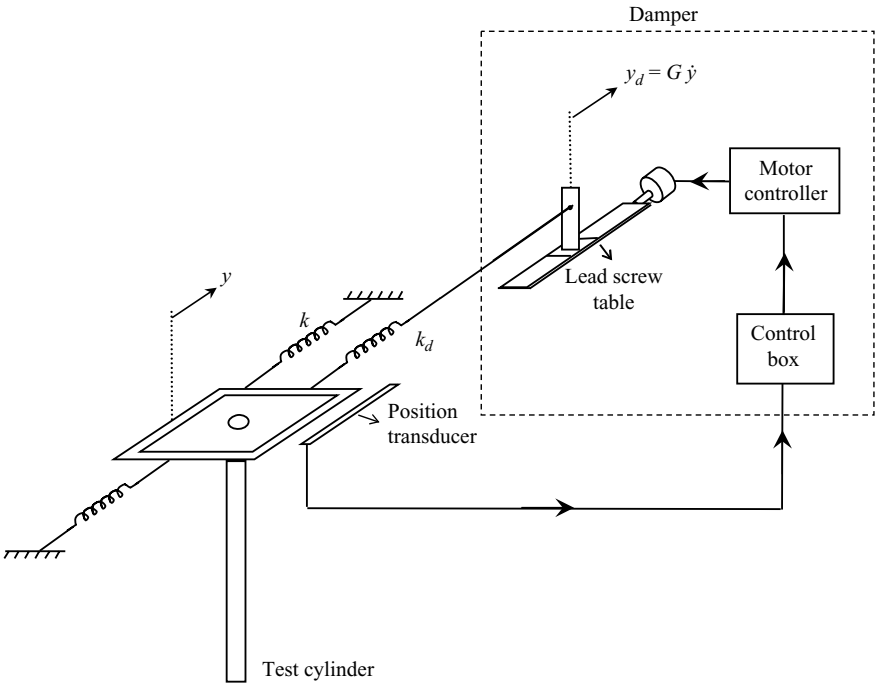

FIGURE 5. Schematic of the active negative–positive damper arrangement. The damper operates by applying a force on the system proportional to the cylinder velocity ($\dot{y}$), by displacing (y_d), the base of an independent spring (k_d), in phase with $\dot{y}$, such that $y_d = G\dot{y}$. The gain G can also be made negative by changing the connections to the motor, thus simply enabling both negative and positive additional damping.

placed 2 mm below the bottom of the cylinder (but not in contact with the cylinder), to encourage two-dimensional shedding, as discussed in Khalak & Williamson (1996).

A mechanical damper capable of applying negative and positive damping to the oscillating system was implemented. This damping was in addition to the very low mechanical damping of the air bearings supporting the cylinder. The damper operated essentially by applying a force on the system proportional to the cylinder velocity ($\dot{y}$), which directly changed the effective structural damping of the oscillating system. This system can be seen in the schematic diagram of figure 5. The required additional damping force was applied by moving the base of an independent spring (k_d) in phase with the cylinder velocity ($\dot{y}$). The velocity was obtained from the cylinder displacement (y) that was measured using a non-contact (magnetostrictive) position transducer. A control box differentiated the measured cylinder displacement (y) in real-time, using an op-amp circuit with an adjustable gain (G) and sent the output to the controller, which commanded the motor moving the base of the spring, with displacement $y_d(t)$. The entire loop was analogue, with typical phase lags of less than 2° introduced from the filtering. The equation of motion for the mechanical system in figure 5 is modified from equation (1.1) to become

$$m\ddot{y} + c\dot{y} + ky + k_d(y - y_d) = F. \tag{2.1}$$

With the control box turned on, the displacement (y_d) of the spring support base was completely governed by the cylinder oscillations ($\dot{y}$), so that $y_d = G\dot{y}$, and the

equation of motion of the overall system may be written as

$$m\ddot{y} + (c - Gk_d)\dot{y} + (k + k_d)y = F. \tag{2.2}$$

From the above equation of motion, it is clear that the effective damping (c_e) of the new system is given by

$$c_e = c - G\,k_d \tag{2.3}$$

where the gain G can be accurately set using a potentiometer. Since the damping due to air bearings (c) is very small, reasonably large negative values of effective damping (c_e) were possible. The value of G can be made negative by changing the connections to the motor controlling the spring support base, so that it moves in the opposite sense. The overall level of damping can be further set by choosing an appropriate value of the damping spring (k_d), although one needs to remember that the effective stiffness of the system ($k_e = k + k_d$) is also affected by the damping spring. Although the feedback loop of this damper is reminiscent of the force-feedback loop of Hover *et al.* (1998), it should be noted that there is no feedback of measured fluid forces in our case. Only structural parameters like damping are affected by the present arrangement.

The controlled mechanical damping arrangement was first tested using simple 'pluck' tests to obtain damping characteristics. In these experiments, the water is emptied from the water channel, and the vibrations of the system are in air. An example time trace of cylinder displacement for such a test is shown in figure 6(a). The oscillations initially decay due to the intrinsic mechanical damping of the air bearings. At time $t = t_A$, the damping control is switched on with an effective negative damping that leads to an exponential growth in oscillations. Subsequently, at time $t = t_B$, the control is adjusted to achieve net zero damping, whereupon the amplitude remains constant in time. Finally at $t = t_C$, we impose a net positive damping to rapidly diminish amplitude as a function of time. As shown in figure 6(b), in all cases the logarithm of the oscillation amplitude varies almost linearly with time, indicating that the damping applied is close to a purely viscous ($c\,\dot{y}$) linear type. In summary, the controlled damper system appears to provide very good viscous ($c\,\dot{y}$) type damping. We now have the ability to vary the damping over a wide regime of negative or positive values. This enables the careful determination of the entire Griffin plot in a single experimental arrangement in this paper.

The electromagnetic damper results from GW98 shown in the introduction were obtained with a damper that operated in principle in a manner similar to the present mechanical damper, with the main difference being that the force application was effected by electromagnetic means. The additional damping force (F_d) was generated by pushing a current (I) in phase with cylinder velocity ($\dot{y}$), through a stationary long copper coil, with a moving magnetic arm (attached to the carriage system) that had magnetic lines of strength (B) cutting some length L of the stationary coil. From simple electromagnetics, the additional force exerted on the moving system is given by $F_d = B\,I\,L$. Since the current I is proportional to $\dot{y}$, the additional force F_d on the moving system is proportional to the cylinder velocity ($\dot{y}$). As discussed previously, this additional force, proportional to $\dot{y}$, directly changes the effective damping of the system.

Important concerns regarding experiments on oscillating cylinders are the possible effects of length-to-diameter ratio (L/D) of the test cylinder, and the tunnel blockage percentage. Before starting experiments on the effects of damping, tests on these aspects were performed, where we kept all other parameters like Reynolds number, mass–damping parameter and mass ratio at constant values. Table 2(a) indicates results from tests for variations in L/D, showing no significant effect of L/D on the

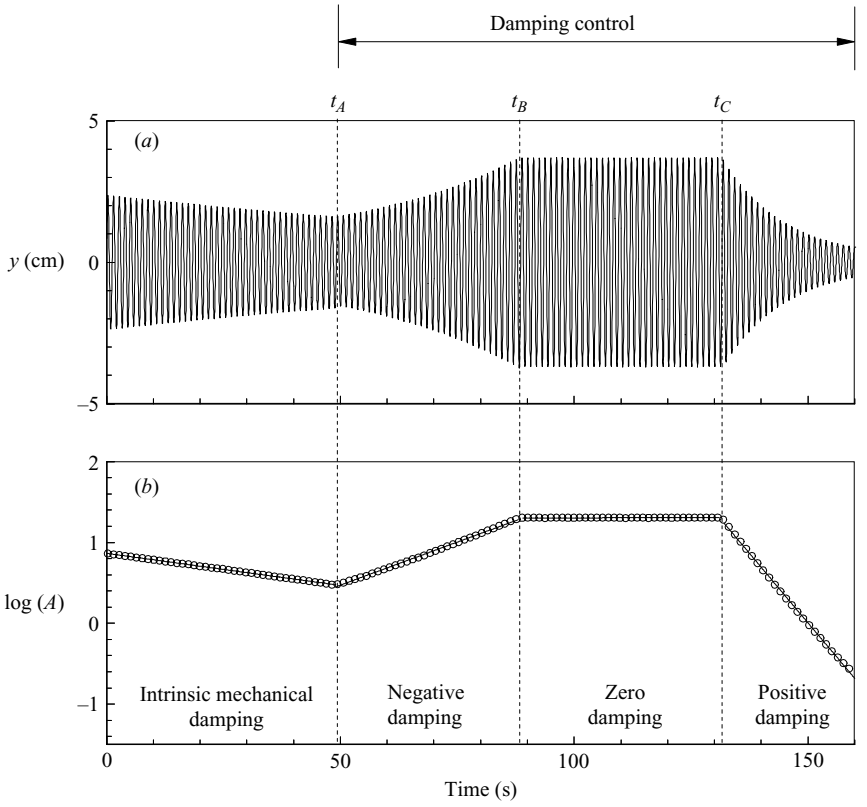

FIGURE 6. Demonstration of effective negative and positive damping control. The damping control is adjusted at times $t = t_A$, $t = t_B$ and $t = t_C$, to change the effective damping of the freely vibrating system to negative, zero or large positive damping, respectively. In all cases, the logarithm of the oscillation amplitude shown in (*b*) varies almost linearly with time, indicating that the applied damping is close to a purely (linear) viscous type ($c\,\dot{y}$). The system vibrates in air only, without the presence of water.

(*a*) L/D	7.2	8.0	12.8	22.67
A^*	0.91	0.89	0.90	0.88
(*b*) D/B	0.05	0.083	0.083	0.133
A^*	0.88	0.91	0.90	0.89

TABLE 2. Effect on peak A^* of varying length-to-diameter (L/D) ratio and tunnel blockage (D/B) ratio, under conditions of zero damping. (*a*) Length-to-diameter (L/D) ratio. (*b*) Tunnel blockage (D/B) ratio. In all cases, experiments were conducted at $Re \approx 4000$, $\alpha = 0$ and $m^* = 10$.

peak amplitude, for L/D in the range of 7 to 22. These experiments were conducted for Reynolds number, $Re \approx 4000$ and mass ratios, $m^* = 10$. For each case, we produced a complete response amplitude plot (A^*), versus normalized velocity (U^*), and the peak value of A^* over the regime of vibrations represents a single data point in table 2(*a*).

Similarly, we find no significant effect of blockage ratio (D/B = diameter/channel width) on peak amplitudes, for blockage less than about 14 %, as may be seen from

table 2(*b*). All subsequent tests for damping presented in this paper were performed with L/D between 7 and 22, and blockage less than 14 %, where peak amplitudes are seen to be nearly unaffected.

The origin of the coordinate system is fixed at the lowest position of the cylinder, at zero flow speed. The x-axis is downstream, the y-axis is perpendicular to the flow direction and to the cylinder axis (defined as transverse), and the z-axis lies along the axis of the cylinder (defined as spanwise). Throughout this paper, we have defined the amplitude to be the average of the top 10 % of the individual amplitude peaks, evaluated over a complete displacement time trace of transverse motion (y/D), in the manner described by Hover *et al.* (1998).

The 'peak amplitude' is the maximum of the amplitudes (defined immediately above) evaluated over a complete amplitude response plot, as normalized velocity is varied (see, for example the bull's eyes in the response plots of figure 3), for a particular mass and damping, and Reynolds number. We shall henceforth refer to this 'peak amplitude' (which is normalized by D) simply as A^*. Throughout this paper, the Reynolds number corresponds to the value Re at peak amplitude conditions in a response plot.

It should be noted that since the oscillations at peak amplitude are not always precisely sinusoidal, measures of amplitude other than the top 10 % measure ($A^*_{10\%}$) used in this paper will yield different numerical values. Analysis of time traces from our data suggests that the maximum amplitude measure (over the complete time trace) typically yields values that are about 7.5 % larger than $A^*_{10\%}$, while the values of the average amplitude measure (A^*_{avg}) and the measure involving the root-mean-square (y_{rms}), where $A^* = \sqrt{2}\,(y_{rms}/D)$, are found to be close to each other and typically about 13 % lower than $A^*_{10\%}$. However, for all the measures the trend with Re and mass–damping is expected, and was found, to be very similar.

3. Mass ratio variation at fixed mass–damping parameter

As described in the Introduction, an important question that has been debated for about 25 years is whether a combined mass–damping parameter (α) could reasonably collapse peak-amplitude data in the Griffin plot. The independent damping control in the present system provides an ideal platform to test this hypothesis directly. We set out to do this by varying mass ratio, keeping the mass–damping parameter and the Reynolds number fixed. The resulting peak amplitudes are plotted in figure 7 as a function of the mass ratio, at two fixed values of mass–damping, namely $\alpha = 0.1$ and 0.5. As may be seen there is no significant effect of mass ratio on the peak amplitudes, for our variation of parameters. Therefore the combined mass–damping parameter should, irrespective of the value of mass ratio, collapse peak-amplitude data on the Griffin plot, as long as other parameters are fixed. This statement is valid at least for mass ratios down to the low value of $m^* = 1$, and is a significant statement, given the long history of this debate.

Earlier, we mentioned that experiments with the electromagnetic damper (GW98) suggested that the amplitude increases as mass ratio decreases. The precise experiments here show that the peak amplitude is independent of mass ratio (for constant α and constant Re). Therefore, we propose that the *variations in peak amplitude in figure 4 are related to changes in Reynolds number rather than mass ratio*. We shall demonstrate this in § 5, after a brief study of the effect of mass–damping on the amplitude response plot in the next section.

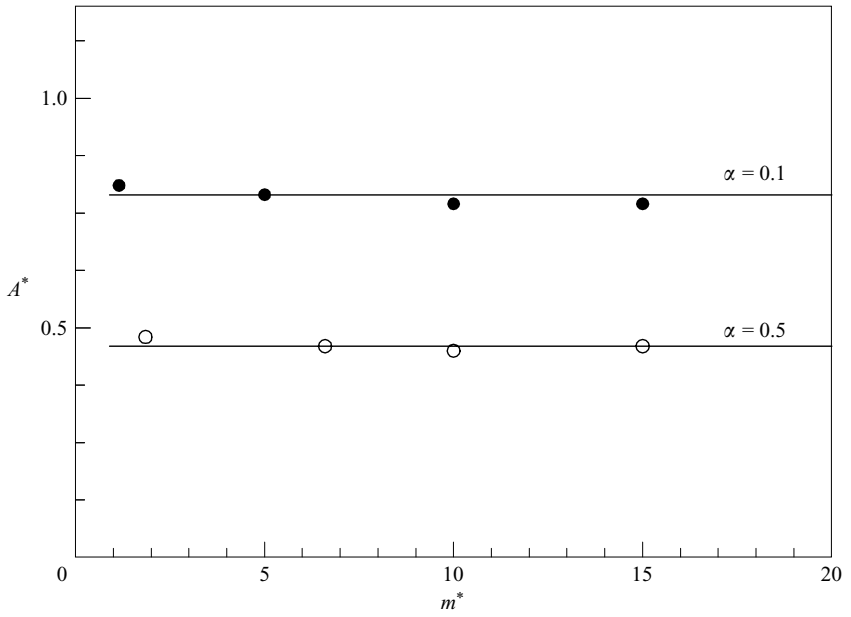

FIGURE 7. Peak response amplitudes (A^*) at a fixed $Re = 4000$ and constant mass–damping (either $\alpha = 0.1$ or 0.5), indicating no significant effect of mass ratio (m^*) over the range of $m^* = 1$–20. This result suggests that a combined mass–damping parameter will collapse peak-amplitude data on the Griffin plot, irrespective of the precise independent values of the mass or damping.

4. Effect of controlled positive and negative damping on amplitude response plots

4.1. *Effect of positive damping on the amplitude response plot: three-branch response versus two-branch response*

A set of amplitude responses, as a function of flow speed, were obtained by systematically increasing the mass–damping parameter from zero, keeping the Reynolds number (corresponding to peak amplitude) fixed at close to $Re = 4000$, and are shown in figure 8. At low mass–damping, the peak amplitude is large and there are three distinct response branches. We see the initial, upper and lower branches in figure 8(*a*). At large mass–damping values as in figure 8(*b*), the upper branch does not occur, and the responses exhibit only two branches. In particular, it appears that the upper branch diminishes as mass–damping is increased, and ceases to exist for amplitudes (A^*) less than about 0.60. This suggests that we may use the condition $A^* = 0.6$ approximately to divide the regimes of three-branch and two-branch response, as it approximately applies over a wide range of Re in this study, and in our previous publications.

The character of the response plot at $Re \approx 4000$ and at other Reynolds numbers is represented in the plane of $\{Re, \alpha\}$ in figure 9. It appears that for each Reynolds number the condition $A^* \approx 0.60$ approximately demarcates the boundary between the two types of response plots. The equation for $A^* \approx 0.60$ in figure 9 was obtained from equation (6.2) below. Interestingly, the trend of the boundary suggests that at low Reynolds numbers, $Re < 500$, only a two-branch response will occur. The data suggest that, when $Re < 500$, even at zero mass–damping, the peak amplitude level never rises sufficiently high (to the level $A^* = 0.6$) to yield an upper branch. In essence,

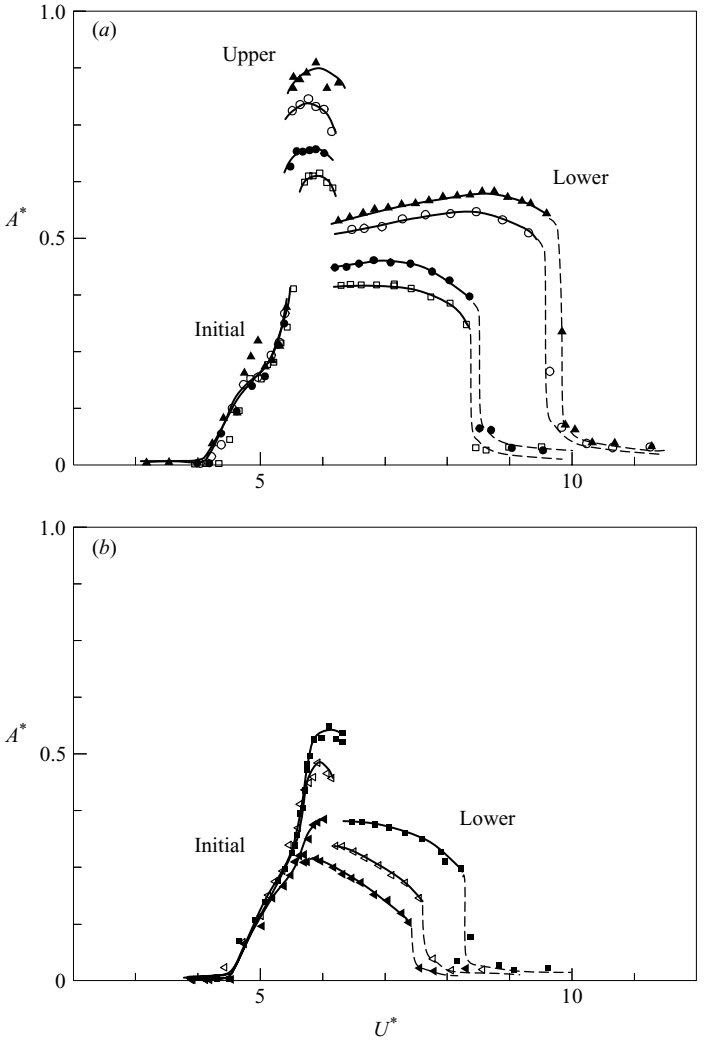

FIGURE 8. Amplitude response plots for increasing mass–damping values (α), at a constant Reynolds number ($Re \approx 4000$). (*a*) Three-branch amplitude responses; (*b*) two-branch amplitude responses. ■, $\alpha = 0.000$; ○, $\alpha = 0.059$; ●, $\alpha = 0.187$; □, $\alpha = 0.252$; ■, $\alpha = 0.340$; ◁, $\alpha = 0.451$; ◀, $\alpha = 0.585$.

at low $Re < 500$, the vibration exhibits only a two-branch response irrespective of the value of mass–damping (α).

4.2. *Effect of negative damping on the amplitude response plot*

We are able to implement reasonably large negative mass–damping on our system, which represents 'structural excitation', as opposed to the more common structural damping. The present brief study appears to be the first one attaining zero damping in an experiment, also enabling response measurements for negative damping.

An example response in figure 10 demonstrates the interesting result that there exists a non-zero amplitude at zero flow speed, $U^* = 0$. In this case, the actual oscillation amplitude is now determined by a balance between the 'mechanical excitation' and the

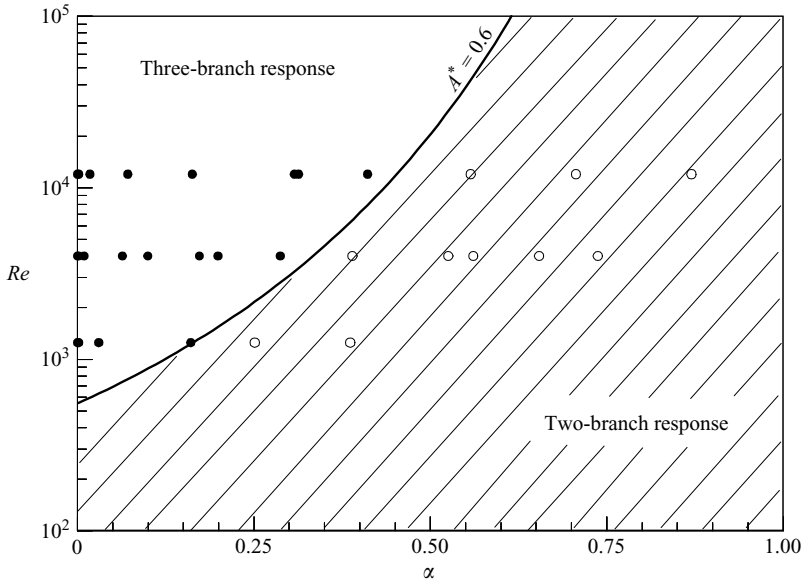

FIGURE 9. Boundary separating the two types of amplitude response (three-branch versus two-branch) in the plane of mass–damping parameter (α) and Re. The line dividing the two regimes is defined by setting $A^* = 0.6$ in equation (6.2), and suggests approximately that below $Re \approx 500$ only the two-branch response will occur, irrespective of the mass–damping value. ●, three-branch response; ○, two-branch response.

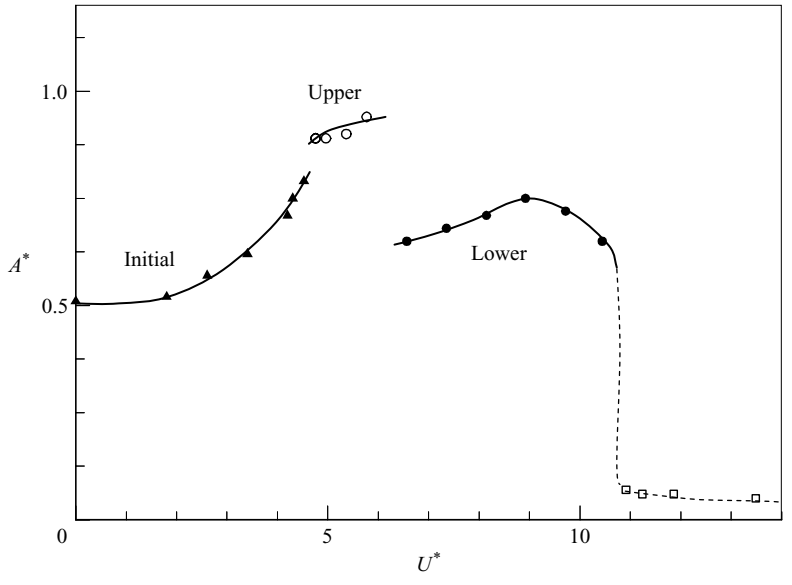

FIGURE 10. A response amplitude plot for negative damping, showing the interesting result that significant oscillation amplitude can occur even at zero flow speed, due to negative mass–damping. Here we have 'structural excitation' and 'fluid damping', which is a complete reversal of roles from the classical situation in vortex-induced vibration, i.e. a balance between fluid excitation and structural damping. At peak A^*, we have $\alpha = -0.133$, $m^* = 10$, $Re = 4000$.

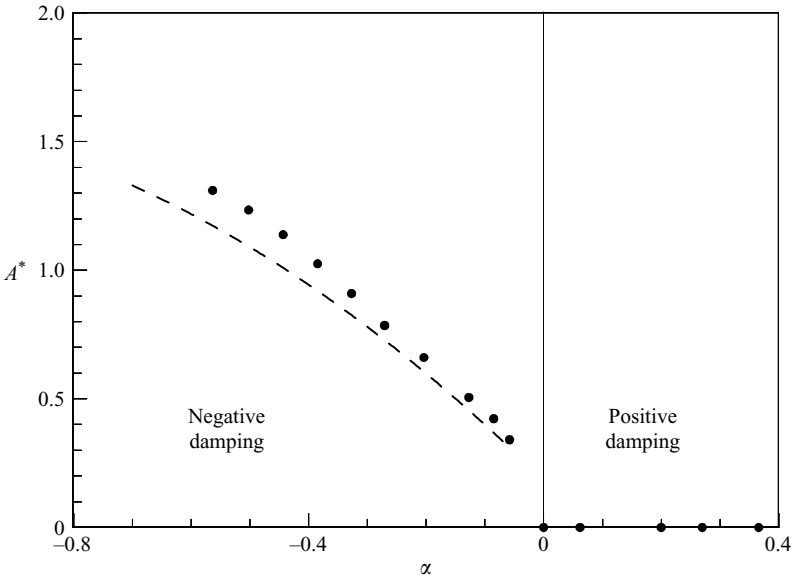

FIGURE 11. Amplitude response (A^*) at zero flow speed ($U^* = 0$) for negative mass–damping. The measured data at negative mass–damping (solid symbols) are predicted well by oscillatory flow (U-tube) force data of Obasaju *et al.* (1988), shown by the dashed line.

'fluid damping', which is a reversal of roles from the classical situation in vortex-induced vibrations, i.e. fluid excitation being balanced by structural damping.

The oscillating cylinder at $U^* = 0$ is essentially similar to the case of a cylinder in an oscillating flow, which has been extensively studied to understand wave loading on offshore structures. The in-line force on a cylinder in oscillatory flow is typically represented by Morison's equation (Morison *et al.* 1950):

$$F = \tfrac{1}{2}\rho D U|U| C_D + \tfrac{1}{4}\pi\rho D^2 \frac{\mathrm{d}U}{\mathrm{d}t} C_M, \tag{4.1}$$

where F is the in-line force per unit length of the cylinder, U is the velocity of the imposed relative motion, and C_D, C_M are drag and inertia coefficients, respectively, that depend on $Kc = 2\pi A/D$ and $\beta = Re/Kc$. By substituting the above fluid force relation into equation (1.1), and noting that the relative motion is equal to the cylinder velocity, i.e. $U = -\dot{y}$, we can obtain the equation of motion for a cylinder at $U^* = 0$ as

$$\left[m + \rho\left(\tfrac{1}{4}\pi D^2\right) C_M\right] \ddot{y} + c\dot{y} + ky = \tfrac{1}{2}\rho D U|U| C_D, \tag{4.2}$$

where the fluid inertia term has been absorbed into the inertial term on the left. The steady-state oscillation amplitude for the above system may be obtained by balancing the energy dissipated per cycle by the fluid damping term on the right with the input energy per cycle from the negative damping term ($c\dot{y}$), assuming the response is sinusoidal, to yield

$$A^* = \frac{3\pi^2}{8} \frac{(-\alpha)}{C_D} \frac{1}{f^*} \tag{4.3}$$

where $f^* = \sqrt{(m^* + 1)/(m^* + C_M)}$. We can predict the oscillation amplitude using experimental data for C_M and C_D, for example using the data of Obasaju, Bearman & Graham (1988). The peak-amplitude response for negative α shows reasonable agreement with such a prediction in figure 11.

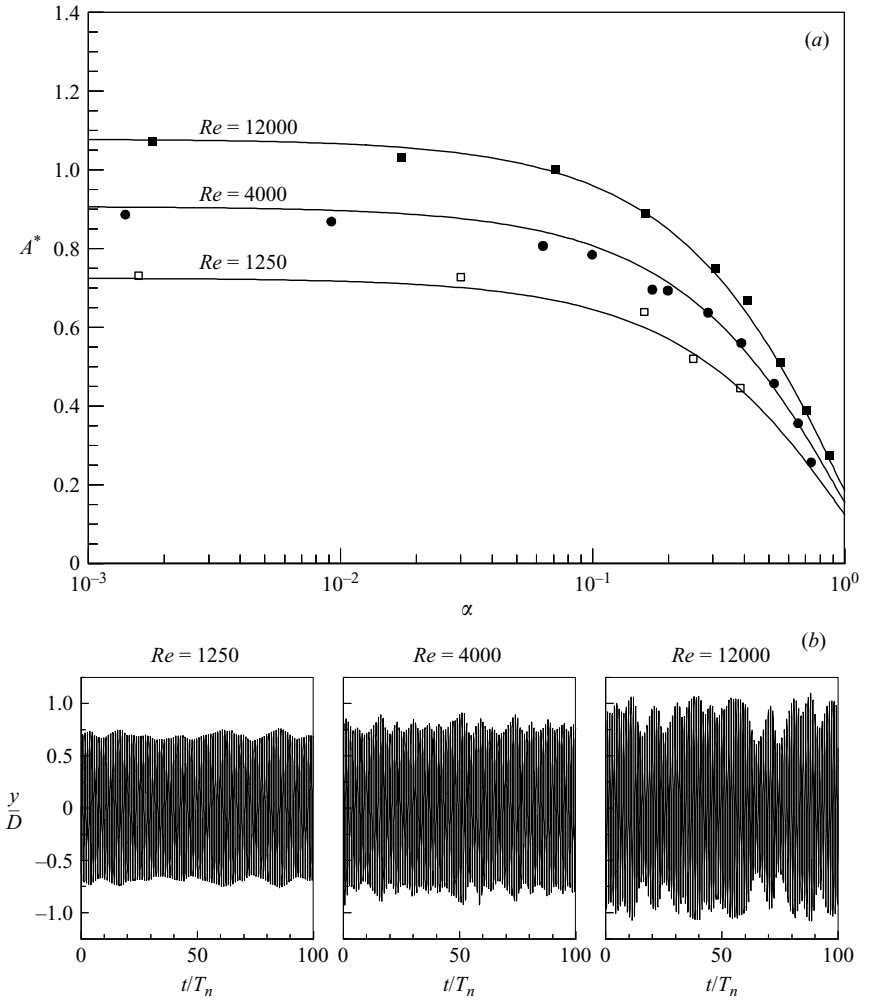

FIGURE 12. Effect of Reynolds number (Re) on peak amplitudes A^*, in the Griffin plot. (a) Curves in the Griffin plot for constant Re; it is immediately clear that an increase in Re causes the complete Griffin plot to shift upwards. (b) Corresponding displacement time traces are shown at zero mass–damping, clearly showing the increase in oscillation amplitudes with Re. In all cases, we keep the mass constant, $m^* = 10$.

5. Effect of Reynolds number on peak response amplitude

In order to investigate the effect of Reynolds number, we determined the peak amplitudes as a function of mass–damping parameter for three different Reynolds numbers, keeping the mass ratio fixed at $m^* = 10$ in all cases. The results shown in figure 12(a) are striking, and show marked variations of the peak amplitude with Re. The effect of Reynolds number on the peak response amplitude is one of the central results of this paper.

Time traces of cylinder oscillations at zero mass–damping, shown in figure 12(b), clearly show the increase in oscillation amplitudes with Re. It should be noted that, in each case, the time traces correspond to the flow speed at which peak oscillation amplitude is found. In addition to the average amplitude increasing with Re, there are also larger fluctuations in amplitude level at higher Re. Essentially, there is an

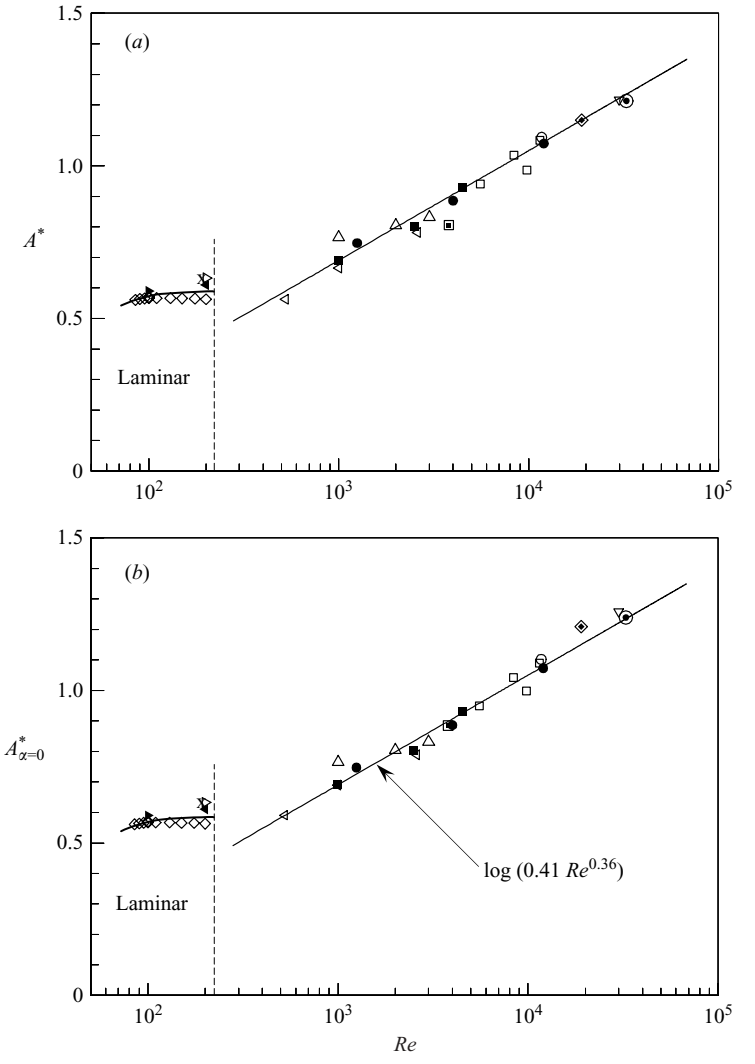

FIGURE 13. Amplitudes (A^*) at very low mass–damping from a number of studies, showing a nearly linear increase versus a logarithmic Reynolds number axis. The computational data shown are at zero mass–damping, while all experimental data, except for ours, are at small but finite mass–damping. In (*b*), the amplitude at zero mass–damping ($A^*_{\alpha=0}$) is determined by extrapolating the relevant data in (*a*) to zero mass–damping using equation (6.1). Symbols correspond to data listed in table 3.

intermittent switching between the upper and lower branch responses, as explained in Khalak & Williamson (1999). The jumps in amplitude are larger at the higher Re, because the upper branch amplitude increases with Re.

One might question the repeatability or validity of our measurements of vibration amplitude. Fortunately, we are in a position to compare precisely the two damping-control techniques we have set up, and as we see in figure 13(*a*), the increase of A^* with Re is highly consistent between the two quite different approaches to control damping. (In the figure, data points obtained with the mechanical damper are shown as ●, and data points obtained with the electro-magnetic damper (GW98) are indicated by ■.)

Source	Medium	Mass–damping (α)	Re (at peak A^*)	Symbol
Present mechanical 'spring' damper	Water	0.000	1250–12 000	●
Present electromagnetic damper (GW98)	Water	0.000	1000–4500	■
Vikestad (1998)	Water	0.019	33 000	⦿
Hover *et al.* (1998)	Water	0.046	3800	⊡
Khalak & Williamson (1999)	Water	<0.01	5500–11 500	□
Govardhan & Williamson (2000)	Water	0.0064	11,700	◯
Smogeli *et al.* (2003)	Water	0.045	19,000	◈
Dahl *et al.* (2004)	Water	0.03	30,000	▽
Klamo *et al.* (2005)	Water	0.007–0.041	525–2600	◁
Lucor (2004)	3D-code	0.000	1000–3000	△
Blackburn & Karniadakis (1993)	2D-code	0.000	200	▷
Newman & Karniadakis (1997)	2D-code	0.000	200	×
Fujarra *et al.* (1998)	2D-code	0.000	200	◀
Shiels *et al.* (2001)	2D-code	0.000	100	▶
Singh & Mittal (2005)	2D-code	0.000	85–200	◇

TABLE 3. Sources for peak-amplitude data at small mass–damping.

This is an important result in that it allows confidence in both the precise effect of Re on amplitude and the success of the two techniques in controlling damping. Another point emerges naturally from this plot: the peak amplitude appears to vary quite linearly with $\log_{10} Re$. One might question whether the results from other investigations, when assembled onto such a plot, may also follow such a linear trend.

A compilation of computational and experimental response data, tabulated in table 3, is plotted as a function of Re in figure 13(a). We note that, unlike the present results, all other experimental data have small but finite mass–damping (α), which leads to slightly lower peak amplitudes than if the damping were zero. We correct for this effect by extrapolating the amplitudes to $\alpha = 0$, using the functional form $A^* = g(\alpha)$ found in equation (6.1) of the next section. The principal point to be made here is that all the peak-amplitude data from all the assembled studies lie, remarkably, along a single straight line when plotted against $\log_{10} Re$ in figure 13(b), and this includes our own data obtained using both the mechanical and electromagnetic damper.

It should be noted that equation (6.1), used to extrapolate amplitudes to the case of $\alpha = 0$, depends on the present data itself, and hence the procedure is iterative, although the values converge rapidly and there is very little difference after two iterations. We should also mention here that we have plotted, in figure 13, only data from the literature, for which the mass–damping is very small, for which Re is readily and precisely evaluated at the conditions of peak amplitude, and for which we are able to precisely evaluate the top 10 % amplitude, A^*, as defined in § 2. The straight line form in figure 13(b) persists down to Re of order 500. For $Re < 200$ the vortex formation is laminar, yielding quite a different relationship, $A^* \sim 0.5$–0.6. (This is only an approximate regime of Re, as the laminar vortex regime is influenced by the vibration of the body, probably extending to slightly higher Re, $Re > 200$.)

These results immediately suggest a good functional form for the data to be $A^* = \log_{10}(B\, Re^C)$. A least-squares fit of all the (non-laminar) data in figure 13(b) for the above functional form, yields best-fit coefficients $B = 0.41$ and $C = 0.36$, thus

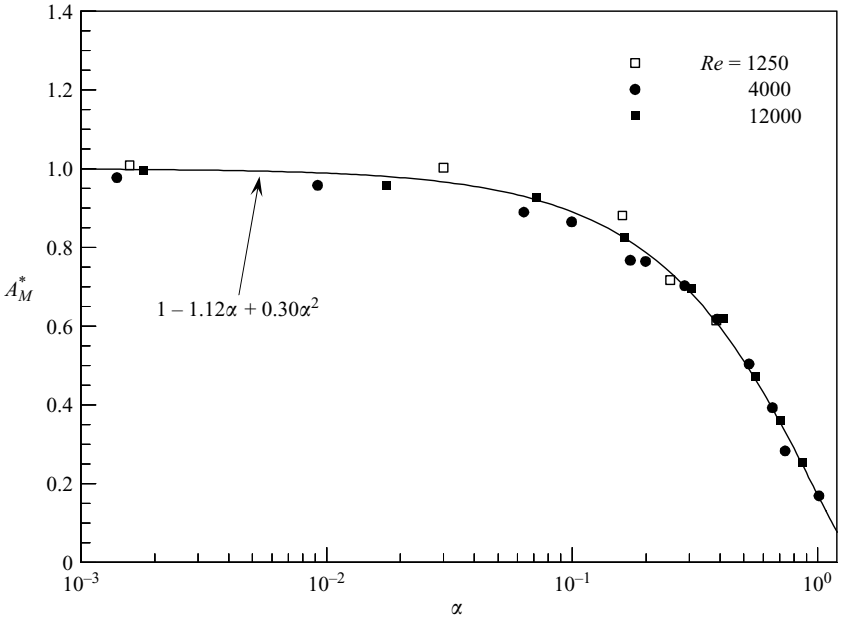

FIGURE 14. The 'modified Griffin plot' obtained using modified peak amplitudes [$A^*_M = A^*/f(Re)$] showing a very good collapse of the different Reynolds number data in figure 12(*a*). This plot, which is now independent of Re, represents the pure effects of mass–damping (α). We recall, from figure 13, that $f(Re) = A^*_{\alpha=0} = \log(0.41\,Re^{0.36})$.

giving the best-fit equation for peak amplitude at zero mass–damping ($\alpha = 0$) as

$$A^*_{\alpha=0} = f(Re) = \log_{10}(0.41\,Re^{0.36}). \tag{5.1}$$

This equation represents the peak-amplitude data in figure 13(*b*) remarkably well, over the entire Reynolds number range of 500 to 33 000, and possibly for higher subcritical Re ($Re < 200\,000$). However, for the fit to be extended beyond about $Re = 40\,000$, it is clear that further measurements are essential. Such experiments are difficult to conduct, because the vibrating structure can become large, and one must be extremely careful to minimize damping (without Coulomb damping), and to properly take account of end conditions with the use of end plates.

We have studied a number of best-fit expressions to represent $f(Re)$, including series expressions in terms of $1/Re$, and also $1/\sqrt{Re}$, amongst other functions. Equation (6.1) has an error of fit that is comparable to the best three-parameter functions, and it is certainly the best of all the two-parameter functions we investigated.

We now return to the variation of A^* with mass–damping for a given Re, as presented in figure 12, using our controlled damping technique. Although the data are significantly displaced for the three different Re, there is a noticeable similarity in their functional behaviour as the mass–damping is increased. This suggests that a normalization using the saturation amplitude at zero mass–damping ($A^*_{\alpha=0}$) from equation (5.1) could collapse the data for the different Re onto a single curve. Figure 14 shows such a 'modified amplitude' $A^*_M = (A^*/A^*_{\alpha=0})$ plotted as a function of mass–damping, indicating a very good collapse of all the different Re data on to a single curve. This 'modified Griffin plot' is now independent of Re, and thus represents the pure effects of the mass–damping parameter (α) on the peak response amplitude.

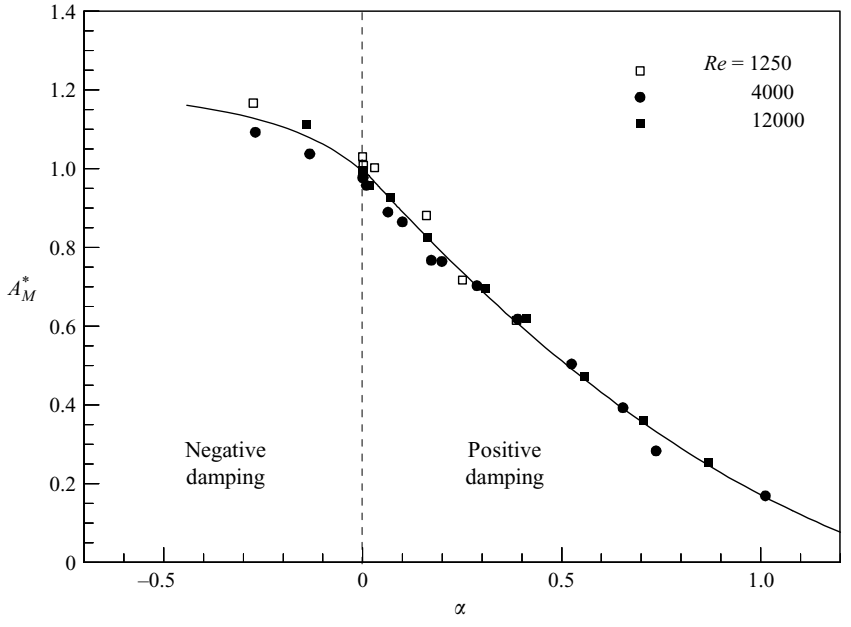

FIGURE 15. Modified Griffin plot using a linear mass–damping (α)-axis, exhibiting results for negative as well as positive damping. Since the present active damping control permits negative damping values, it suggests the use of a linear α-axis. As the mass–damping goes through zero to negative values, the modified amplitude increases smoothly, indicating that small variations in mass–damping around $\alpha = 0$ will lead to almost no change in amplitude, as seen by the existence of the saturation amplitude in figure 14.

The modified Griffin plot in figure 14 shows clearly that a saturation amplitude is reached at small mass–damping. The concept of a saturation of the peak amplitudes is not surprising, and has been discussed previously in many papers. In the present work, we can reduce the net damping to exactly zero or even take it to negative values of α, suggesting that the data may be better represented on a linear mass–damping axis, as shown in figure 15. In this case, we find that as the mass–damping is reduced continuously through zero to negative values, the amplitude also increases continuously (not surprisingly). It is clear from the nature of the data in figure 15 that there should be very little difference between A^* at small mass–damping of the order of 0.01 and A^* for exactly zero mass–damping, which is also exhibited by the saturation amplitude levels in figure 14. With the present technique, we can make the damping strongly negative, implying that we are actually mechanically exciting the cylinder to vibrate, as discussed in § 4.2.

The modified Griffin plots of figures 14 and 15 are important as they represent single curves that completely define the effect of mass–damping, valid for our Re regime compiled here, and possibly extending well beyond this regime. We shall now propose functional fits to represent the effect of α, as well as the effect of Re, on A^*.

6. Defining a new functional relationship: $A^* = A^*\{Re, \alpha\}$

Equations to fit compiled data in the classical Griffin plot, for example figure 1(a), have been put forward by several investigators, whose empirical functions are listed in Blevins (1990, table 3-2). Given the large scatter in the data due in large part to the

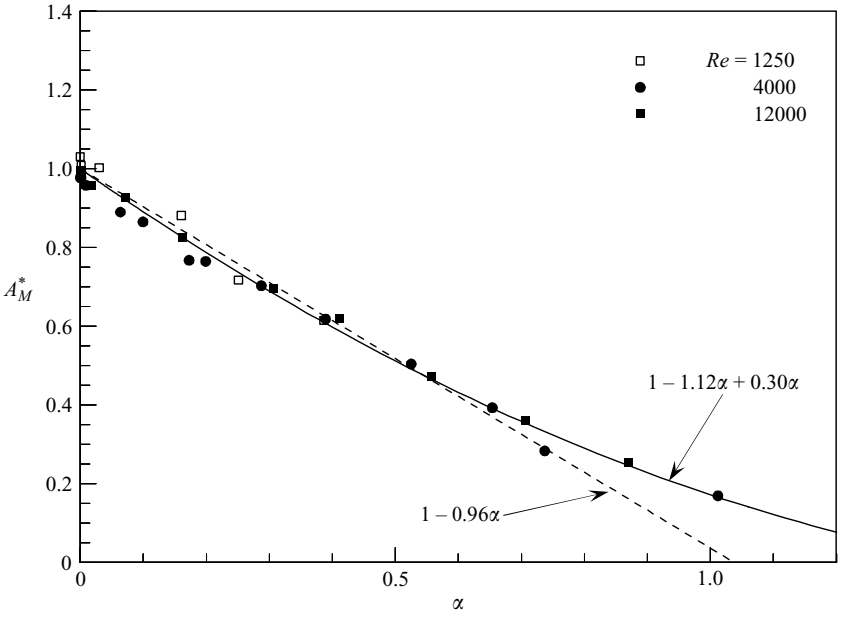

FIGURE 16. Linear and quadratic relationships to represent variation of modified amplitude (A^*_M). A simple linear function, $A^*_M = 1 - 0.96\,\alpha$, fits the modified amplitude data remarkably well, for $\alpha < 0.75$. The fit is compared with the quadratic $A^*_M = (1 - 1.12\,\alpha + 0.30\,\alpha^2)$.

effects of Reynolds number, it is difficult to select one functional relationship rather than another. However, the present data in the modified Griffin plot of figures 14 and 15, may be used to indicate an overall functional relationship between $\{A^*,\ Re,\ \alpha\}$.

We present in Appendix B, table 4, a number of different functional forms including those that have been employed in the literature. Interestingly, we find that a simple quadratic function of the form $A^*_M = 1 + B\alpha + C\alpha^2$, with only two coefficients, has the least error of fit (based on the data in figure 14), for mass–damping values ranging from zero to unity $(0 < \alpha < 1)$:

$$A^*_M = A^*/A^*_{\alpha=0} = g(\alpha) = 1 - 1.12\,\alpha + 0.30\,\alpha^2. \tag{6.1}$$

This relationship $g(\alpha)$ fits the collapsed data in figure 16 very well, over the regime $(0 < \alpha < 1)$. We can now put forward an equation for the peak response amplitude, as a function of mass–damping $g(\alpha)$, and Reynolds number $f(Re)$, as follows:

$$\begin{aligned} A^* &= g(\alpha)\, f(Re), \\ A^* &= [1 - 1.12\,\alpha + 0.30\,\alpha^2]\, \log_{10}(0.41\, Re^{0.36}). \end{aligned} \tag{6.2}$$

One should note that such a quadratic relationship for $g(\alpha)$ cannot represent the response well for very low amplitudes of order $A^* \sim 0.1$, found at much larger mass–damping, because the function $g(\alpha)$ ultimately rises (when α exceeds 1.87). However, in this work we are concerned with the regime where $A^* > 0.1$, which is above the threshold where one expects lock-in between vortex dynamics and body motion, and which is represented by the mass–damping regime $\alpha < 1.2$, shown in figure 16.

It is also possible, without much loss in accuracy, to represent the data for $\alpha < 0.75$ by a linear function $g(\alpha)$, yielding the following expression:

$$A^* = [1 - 0.96\,\alpha]\, \log_{10}(0.41\, Re^{0.36}), \tag{6.3}$$

which is shown as the dashed line in figure 16. The errors associated with the linear and quadratic functions $g(\alpha)$ are included in Appendix B, table 5. In cases where the body is in water, the mass–damping is typically small, so that a good estimate is given by the linear representation in (6.3).

As a final point, the close representation of the data by a linear fit may be of significance to wind engineering applications. Several semi-empirical models of the interaction between body motion and fluid forcing have been put forward (see Parkinson 1989). For example, Vickery (1990) characterized the velocity-correlated forces as a negative self-limiting aerodynamic damping. Our results would suggest a linear relationship between such damping and these high motion amplitudes, and corresponds with similar experimental support for a linear relationship at lower amplitudes from Blackburn & Melbourne (1993). By using Vickery's equation (5) one finds a good representation of our amplitude data. Further work in this direction might be useful, but is outside the scope of this study.

Finally, it may be noted that there is no significant effect of Reynolds number on the amplitudes measured for the lower branch, over a wide regime of Re, or for vortex-induced vibrations in the laminar regime ($Re < 200$), both of which are presented in Griffin plots in Appendix A.

7. The collapse of data in the 'modified Griffin plot' and the introduction of design curves

We now return to the fundamental question of why there is a large degree of scatter in the conventional Griffin plot, as shown typically in figure 1. Given the collapse of our own data using the modified amplitude, A^*_M, taking into account the effect of Re, it is clear that one should investigate whether such a collapse will ensue with the collected peak-amplitude data from these and other studies.

We begin with a plot of our compiled amplitude data (A^*) in figure 17, showing a large scatter. (We plot here only those data for which we have an accurate measure of Re at the maximum amplitude condition, a precise measure of top 10% amplitude, and for which the experiments have employed endplates.) It is not surprising that one cannot validate one best-fit functional curve through these data, in preference to any other curve. If one now replots the data, using instead the modified amplitude $A^*_M = A^*/f(Re)$, then we find the data collapses beautifully onto a single curve. A good representation of this curve is given by our equation (6.1):

$$A^*_M = g(\alpha) = 1 - 1.12\,\alpha + 0.30\,\alpha^2.$$

Rather than conventionally consider only one curve through a large scatter of data, we may now construct 'design curves', each one corresponding to a chosen Reynolds number, as presented in figure 18. These design curves enable one to very simply determine, using a graphical approach, expected peak response for given $\{\alpha,\ Re\}$. These design curves and equations (6.1) and (6.2) have been based on data in the Reynolds number range from about 500 to 33 000. Although one could expect this trend to continue to higher subcritical Re, it is clear that it cannot continue indefinitely. Whether the trend persists to the upper limit of the subcritical regime, or tails off in advance of this Reynolds number ($Re \sim 200\,000$), is not known. Our results certainly point to the importance of assembling peak-amplitude data at much higher Re. However, such experiments will be challenging, because it is essential to properly arrange the cylinder end conditions, in a 'clean' incident flow, and especially to precisely design for minimum (or zero) linear damping, without Coulomb friction.

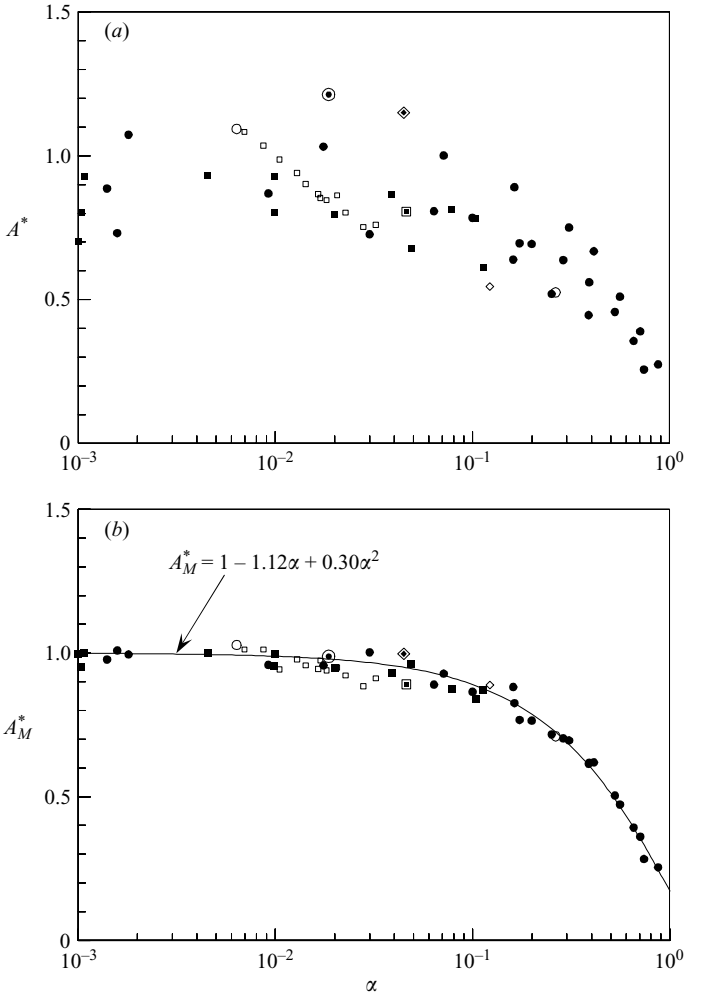

FIGURE 17. Collapse of previously scattered data from the Griffin plot, by taking into account Reynolds number. If we replot all of the data in the 'modified Griffin plot' in (*b*), employing our 'modified amplitude' $[A^*_M = A^*/f(Re)]$, all of the data collapses beautifully onto a single curve. ●, Mechanical 'spring' damper; ■, Electromagnetic damper; ⦿,Vikestad (1998); ⊡, Hover *et al.* (1998); □, Khalak & Williamson (1999); ○, Govardhan & Williamson (2000); ◇, Blackburn *et al.* (2001); ◈, Smogeli *et al.* (2003); —, present curve fit: $A^*_M = (1 - 1.12\alpha + 0.30\alpha^2)$.

Finally, by way of illustration, we choose case studies of response data in figure 19 (over a range $Re = 1260$–$32\,700$). These data have been extracted from facilities in different institutions, comprising both water channel and towing tank data. In each case, the peak-amplitude data are predicted well by the design curve at the appropriate Re. One can immediately appreciate the fact that, without account of Reynolds number, the selected data in figure 19 would be widely scattered, whereas in fact these data lie close to their Griffin plot curves corresponding to their respective Reynolds numbers.

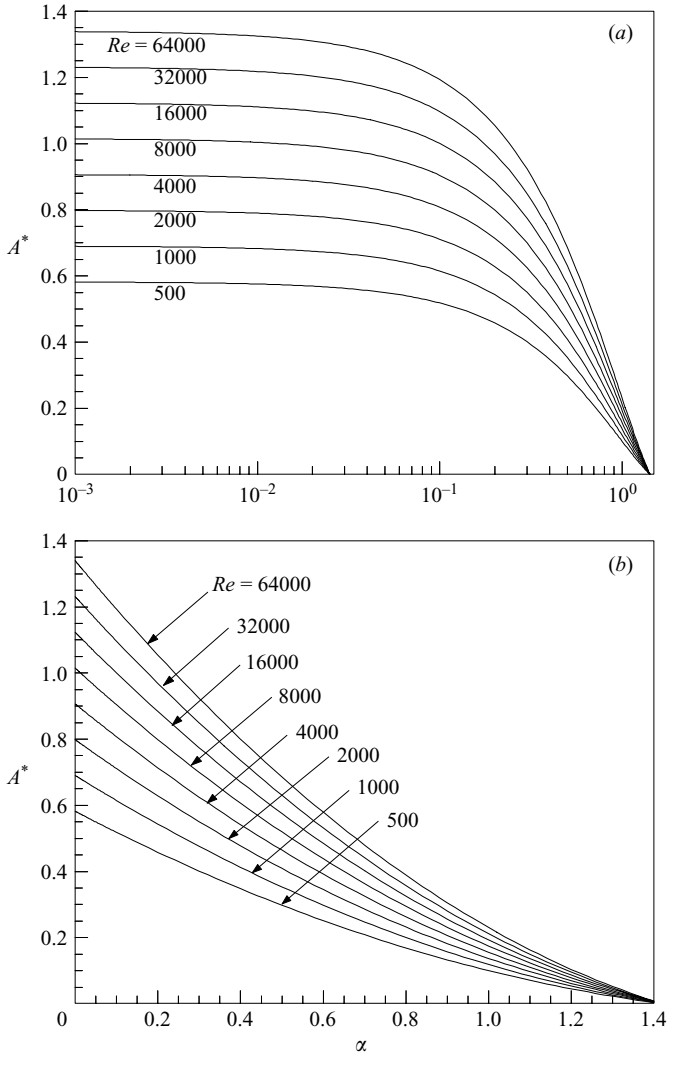

FIGURE 18. 'Design curves' of peak amplitude on the Griffin plot. Each curve for constant Re, is drawn using equation (6.2), and shows again the marked effect of Re on the Griffin plot. These design curves permit rapid estimation of the peak amplitude for given Re and mass–damping. In (a), the mass–damping axis is logarithmic and in (b), the axis is linear. The latter plot of the data is perhaps the most useful format. The plot should be used in the regime $\alpha < 1.2$.

8. Concluding remarks

We have implemented methods to control both negative and positive mechanical damping in a system comprising the transverse vortex-induced vibrations of an elastically mounted rigid cylinder in a fluid flow. This has enabled us to systematically study the variation of peak amplitude response (A^*) as a function of mass–damping (α), in the so-called 'Griffin plot'.

Our early investigations in 1998, using an electromagnetic damper, apparently showed that the peak response level was pushed higher as mass ratio (m^*) was decreased, even when α was kept constant. By using a second method to control damping, we now show this unexpected result to be a coincidence. The present

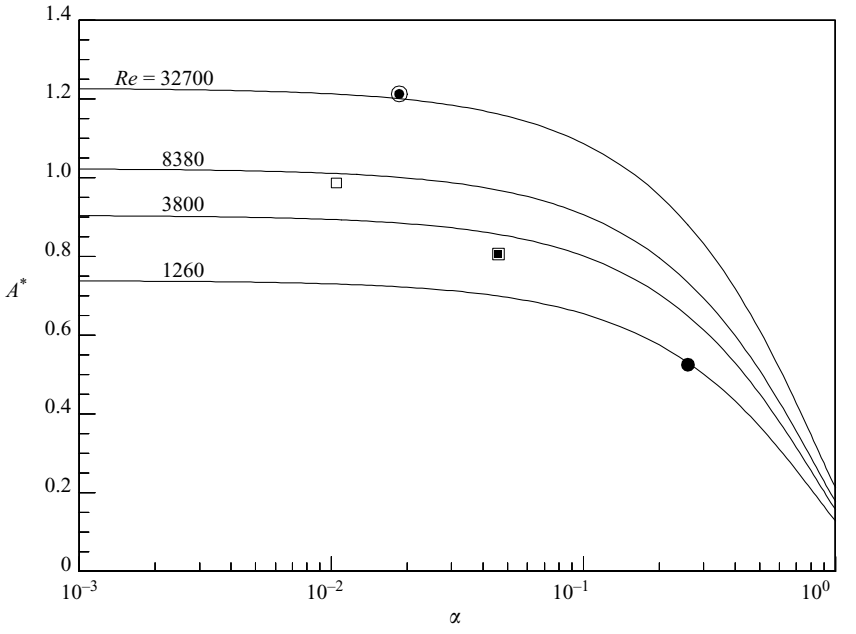

FIGURE 19. Case studies demonstrating the use of the Griffin curves. Previously scattered data can now be assigned to their specific Reynolds number curves, in these cases over the regime $Re = 1\,000$–$33\,000$. The data chosen here are selected from those plotted in figure 17, and correspond to water channel and towing tank facilities. They represent three quite diverse approaches to VIV: elastically mounted vertical cylinders in a water channel (Cornell); elastically mounted horizontal cylinder translated along a towing tank (Marintek, Norway); a 'controlled' horizontal cylinder in a towing tank, using the Virtual Cable Testing Apparatus (MIT). ●, Govardhan & Williamson (2000); ⊡, Hover *et al.* (1998); □, Khalak & Williamson (1999); ⦿, Vikestad (1998).

technique of control employs a spring whose base is displaced precisely in phase, or out of phase, with the body's velocity. Generally, to achieve low mass–damping in experiments, one typically decreases the mass ratio, and this may be done by increasing the cylinder diameter. However, this simultaneously increases the Reynolds number. We show clearly in this paper that it is the variation of this parameter, Re, rather than changes in the mass ratio itself, that causes the peak amplitude to rise.

The fact that an increase in Reynolds number corresponds with an increase in peak-amplitude response in a VIV system is a result that may be expected, based on the force measurements at MIT under Michael Triantafyllou and Franz Hover. For bodies in controlled transverse vibration, they showed that a regime of positive excitation could be found up to higher amplitudes, when Re is increased (up to $Re \sim 19\,000$) in Smogeli (2002), and these results were presented by Triantafyllou *et al.* (2004). In a study, independent of our own, the group at Caltech have shown the general trend of an increase of peak amplitudes for vortex-induced vibration as Re increases, presented in Klamo *et al.* (2004). In their subsequent paper (Klamo *et al.* 2005), they state that 'the Reynolds number, which has generally been ignored in discussions of maximum amplitude data, is an important parameter'. Clearly, this statement is in direct accordance with our results in this paper.

By examining our results and those from many previous experiments for lightly damped systems, over a range of Reynolds numbers, $Re = 500$–$33\,000$, we find that the peak-amplitude data increase nearly linearly versus a logarithmic Reynolds number

axis. Peak-amplitudes corresponding to zero damping ($A^*_{\alpha=0}$) are very well represented by the functional form

$$A^*_{\alpha=0} = f(Re) = \log(0.41\, Re^{0.36}).$$

Despite the significant effect of Re on peak amplitudes, the variation of A^* with mass–damping is proportional to a function $g(\alpha)$, which is found to be remarkably independent of Re. We are thus in a position to separate the variables, and to propose that the amplitude is given by $A^* = g(\alpha)\, f(Re)$ presented in equation (6.2):

$$A^* = (1 - 1.12\,\alpha + 0.30\,\alpha^2)\, \log(0.41\ Re^{0.36}).$$

Over a regime of mass–damping, $\alpha < 0.75$, which corresponds with amplitudes A^*_M greater than 0.3, a very good representation of the peak amplitudes is actually given by a linear variation of $g(\alpha)$ in equation (6.3):

$$A^* = (1 - 0.96\,\alpha)\, \log(0.41\, Re^{0.36}).$$

The significant effect of Reynolds number on peak vibration amplitudes, that we observe in this study, should be linked to changes in the near-wake vortex dynamics that are responsible for the body motion. In the case of the stationary cylinder in a flow, a compilation of lift coefficient (C_L) data by Norberg (2003) shows a substantial increase in C_L values over the Re range from 1000 to 200 000. This Re range falls in the 'shear layer transition' regime as discussed in Roshko (1993) and in Williamson (1996), where the size of the wake formation region decreases and there is a general increase in the two-dimensional Reynolds stress levels. The above variations are consistent with more coherent vortices forming closer to the cylinder, which would yield a larger lift force, and possibly greater amplitude in the case of the vibrating body. However, there is clearly a difference between the upper branch response, which yields the peak amplitude (which is influenced by Re), and the lower branch response, whose amplitude is reasonably Re independent. One might conclude that the physical cause of the Reynolds number effects, presented in this paper, remain an open and interesting question.

In this paper, we have assembled a complete plot of previous amplitude data (A^*), measured over the last 30 years, versus mass–damping (α), which shows a large scatter. One should therefore not be surprised that investigators have had difficulty validating a unique functional relationship for such data. (In fact, opinions as to whether a combined mass–damping parameter works well, or does not work, cannot be supported by the data one way or the other in the light of this large scatter.) However, if one now replots the data instead using the 'modified amplitude', $A^*_M = A^*/f(Re)$, then all the previous data collapse beautifully onto a single curve $g(\alpha)$ in this 'modified Griffin plot', given by

$$A^*_M = (1 - 1.12\,\alpha + 0.30\,\alpha^2).$$

One may also construct a family of 'design curves', each one corresponding to a chosen Reynolds number, in the Griffin plot. Although these results have been developed for the Re range 500–33 000, there remains a need to investigate whether further increases in amplitude will occur at higher subcritical Re, if similar experimental arrangements are employed. At higher Reynolds numbers, corresponding to the drag crisis, and in the supercritical regime ($Re > 200\,000$), one must expect substantial variations of the parameters, with a greater sensitivity

to surface roughness and free-stream turbulence, for example. Further experiments at high Re are possible in large facilities, such as at MIT, and at the Institute for Marine Dynamics in Newfoundland, amongst other facilities.

There has also been much debate over the last three decades concerning the validity of using the product of mass and damping in these problems, although precise experiments to investigate this point have not been readily available. Our results here, made possible by the controlled damping, indicate that the combined mass–damping parameter (α) does indeed collapse peak-amplitude data well, at a given Re, independent of the precise mass and damping values, for a wide regime of mass ratios even extending down to $m^* = 1$.

Finally, employing our technique to control the damping, we also obtain amplitude responses for negative mass–damping values, which exhibit significant vibration even at zero normalized flow speed, $U^* = 0$. These response amplitudes are predicted well by experiments for a cylinder in oscillatory flow of the type used in offshore wave–structure studies.

The support from the Ocean Engineering Division of ONR, monitored by Dr Tom Swean, is gratefully acknowledged (ONR Contract Nos. N00014-04-1-0031 and N00014-95-1-0332). Although the original experiments were started in 1998 using the electro-magnetic technique, the principal experiments with the mechanical 'spring' damper were initiated in 2000–2001 (during a postdoctoral appointment of R.N.G. at Cornell), and the experiments were subsequently conducted during two summer visits from India to Cornell by R.N.G. in summer 2002 and 2003. All the experimental work reported within this paper was completed by July 2003. (Earlier completion of the manuscript text was held up by refusal of a travel visa for a planned R.N.G. visit in Summer 2004.) Our thanks are especially due to Dr Nathan Jauvtis, who, with R.N.G., first deduced and plotted the variation of amplitude with Re in 2001. We also thank the NASA Space Grant Consortium for their Fellowship support of Josh Conlon for his summer undergraduate project in June-July 2003, where he diligently explored the curve fits for $f(Re)$ and $g(\alpha)$, and assembled data sets from external sources. Thanks are also due to Kyrre Vikestad for sharing his time traces, and for enthusiastically computing his top 10% amplitude levels for a key data point at high Re in October 2003. We thank Michael Triantafyllou and Franz Hover, as well as Jason Dahl, for sharing their results, and for discussions on effects of Re in 2003, and for making the work of Smogeli (2002) known to us. Finally, we acknowledge the Caltech Team of Joe Klamo, Tony Leonard and Anatol Roshko for their presentation at the APS meeting in November 2004, where they made a strong and important point regarding the significance of Reynolds number in these VIV problems. We would particularly like to acknowledge the enthusiastic communication between C.H.K.W. and Joe Klamo at the meeting. Aside from discussions of how to characterise amplitude, one key outcome was the addition of three further data points to add to our figure 13, extending the data down to $Re = 525$, for which we are most grateful.

Appendix A. Griffin plot for the lower branch and the laminar regime

A.1. *Griffin plot for the lower branch*

In the case of the lower branch, the displacement time traces of figure 20, for zero α suggest that the amplitude level is independent of Re, over at least a regime,

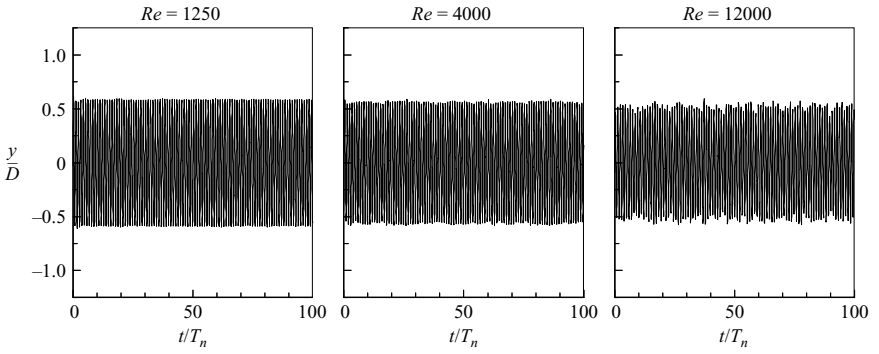

FIGURE 20. Displacement time traces in the Lower branch, showing no significant effect of Re, in contrast to the character of the Upper branch (see figure 12b). In all cases, the mass–damping parameter is zero ($\alpha = 0$), and the mass ratio, $m^* = 10$.

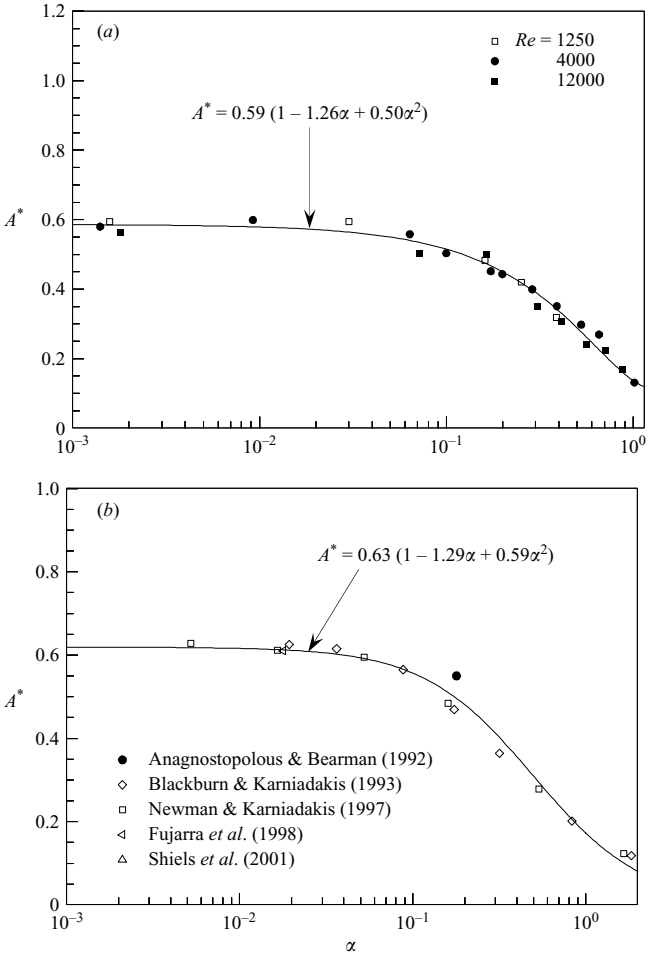

FIGURE 21. Griffin plots for the lower branch and for the laminar regime. (a) Peak-amplitudes (A^*) in the lower branch at three different Re showing that the lower branch is nearly independent of Re. (b) Peak-amplitudes in the laminar regime (data is for $Re \leqslant 200$) from several investigators show good agreement, exhibiting also a saturation amplitude $A* \sim 0.6$ for very small or zero α. In both cases, the collapsed data are represented well by a quadratic function of α.

$Re = 1250$–$12\,000$. This is further demonstrated by the Griffin plot representation in figure 21(*a*), where the data for different Re collapse onto the same curve (unlike the data for the upper branch in figure 12), and are represented well by the best-fit curve

$$A^* = 0.59\,[1 - 1.26\alpha + 0.50\alpha^2]. \tag{A 1}$$

A.2. *Griffin plot for the laminar regime*

In the laminar Reynolds number regime, peak response amplitudes for zero damping are nearly independent of Re, over the Re range from about 85 to 200, as shown by the data of Singh & Mittal (2005) in figure 13. In fact, it appears that peak-amplitude data in the Griffin plot are represented well by a single curve in figure 21(*b*), using data from a number of computational and experimental studies. We obtain the best-fit equation for peak response amplitude in this laminar regime as

$$A^* = 0.63\,[1 - 1.29\,\alpha + 0.59\alpha^2\,]. \tag{A 2}$$

Appendix B. Tables showing various functional representations for A^*_M as a function of α.

	Investigation	Function	Best-fit coefficients	Error of fit
(1)	Present	$A^*_M = 1 + B\,\alpha + C\,\alpha^2$	B = −1.1241 C = 0.2960	0.000623
(2)	Blevins (1977)	$A^*_M = \dfrac{B}{C+\alpha}\sqrt{\left(D + \dfrac{E}{C+\alpha}\right)}$	B = 3.5219 C = 1.8203 D = −0.4371 E = 1.2814	0.000690
(3)	Present	$A^*_M = \mathrm{e}^{B\,\alpha}$	B = −1.3763	0.001308
(4)	Present	$A^*_M = 1 + B\,\alpha$	B = −0.9156	0.001480
(5)	Griffin & Ramberg (1982)	$A^*_M = B/(1 + C\,\alpha)^D$	B = 1.0130 C = 0.1609 D = 9.1045	0.001493
(6)	Sarpkaya (1978)	$A^*_M = B/(\sqrt{C + \alpha^2})$	B = 0.2788 C = 0.0828	0.001671

TABLE 4. Comparison of fits employed by various investigators for peak amplitude versus mass–damping (based on all data in figure 16).

	Investigation	Function	Best-fit coefficients	Error of fit
(1)	Present	$A^*_M = 1 + B\,\alpha$	B = −0.9636	0.000878
(2)	Present	$A^*_M = 1 + B\,\alpha + C\,\alpha^2$	B = −1.1031 C = 0.2513	0.000658

TABLE 5. Comparison of linear and quadratic fits to represent peak-amplitude data, for the regime $\alpha < 0.75$ (based on data in figure 16).

REFERENCES

Anagnostopoulos, P. (Ed.) 2002 *Flow-Induced Vibrations in Engineering Practice*. Ashurst, UK: WIT Press.

Anagnostopoulos, P. & Bearman. P. W. 1992 Response characteristics of a vortex-excited cylinder at low Reynolds numbers. *J. Fluid Struct*. **6**, 39–50.

Anand, N. M. & Torum, A. 1985 Free span vibration of submerged pipelines in steady flow and waves. In *Proc. Intl Symp. Separated Flow Around Mar. Struct*., pp. 155–99. Trondheim, Norway.

Angrilli, F., Di Silvio, G. & Zanardo, A. 1972 Hydroelasticity study of a circular cylinder in a water stream. In *Flow-Induced Structural Vibrations* (ed. E. Naudascher), pp. 504–512. Springer.

Bearman, P. W. 1984 Vortex shedding from oscillating bluff bodies. *Annu. Rev. Fluid Mech.* **16**, 195–222.

Blackburn, H. M., Govardhan, R. N. & Williamson, C. H. K. 2001 A complementary numerical and physical investigation of vortex-induced vibration. *J. Fluids Struct*. **15**, 481–488.

Blackburn, H. & Karniadakis, G. E. 1993 Two and three-dimensional simulations of vortex-induced vibration of a circular cylinder. In *Proc. 3rd Intl Offshore Polar Engng Conf*., pp. 715–720.

Blackburn, H. M. & Melbourne, W. H. 1993 Cross flow response of slender circular-cylindrical structures: Prediction models and recent experimental results. *J. Wind Engng Ind. Aerodyn.* **49**, 167–176.

Blevins, R. D. 1990 *Flow-Induced Vibrations*. Van Nostrand Reinhold.

Dahl, J. M., Hover, F. S. & Triantafyllou, M. S. 2004 Two degree of freedom vortex induced vibrations of a circular cylinder in subcritical flow conditions. *Proc. 8th Intl Conf. on Flow-induced Vibration, FIV 2004, Paris, France, 6–9 July*, (ed. E. de Langre & F. Axisa), Vol. II, pp. 303–320.

Feng, C. C. 1968 The measurements of vortex-induced effects in flow past a stationary and oscillating circular and D-section cylinders. Master's thesis, University of British Columbia, Vancouver, BC, Canada.

Fujarra, A. L. C., Meneghini, J. R., Pesce, C. P. & Parra P. H. C. C. 1998 An investigation of vortex-induced vibration of a circular cylinder in water. *Proc. Conf. on Bluff Body Wakes and Vortex-Induced Vibrations, Washington, DC, 21–23 June, Paper* 25. Printed at Cornell University, NY. Also Paper FEDSM98-5195, in ASME CD-ROM of Fluids Engng Summer Meeting, FEDSM98.

Gharib, M. R., Leonard, A., Gharib, M. & Roshko, A. 1998 The absence of lock-in and the role of mass ratio. *Paper* FEDSM98-5312, CD-ROM. *ASME Fluids Engineering Summer Meeting*, FEDSM98.

Govardhan, R. & Williamson, C. H. K. 2000 Modes of vortex formation and frequency response of a freely vibrating cylinder. *J. Fluid Mech.* **420**, 85–130.

Govardhan, R. N. & Williamson, C. H. K. 2005 Revealing the effect of Reynolds number on vortex-induced vibrations using controlled negative and positive damping. In *Proc. Fourth Conf. on Bluff Body Wakes and Vortex-Induced Vibrations (BBVIV4), 21–24 June 2005, Santorini, Greece* (ed. T. Leweke & C. H. K. Williamson), pp. 69–71.

Griffin, O. M. 1980 Vortex-excited cross-flow vibrations of a single cylindrical tube. *ASME J. Pressure Vessel Technol.* **102**, 158–166.

Griffin, O. M. & Ramberg, S. E. 1982 Some recent studies of vortex shedding with application to marine tubulars and risers. *ASME J. Energy Resour. Technol.* **104**, 2–13.

Griffin, O. M., Skop, R. A. & Ramberg, S. E. 1975 The resonant vortex-excited vibrations of structures and cable systems. In *7th Offshore Technol. Conf., Houston, TX, OTC Paper* 2319.

Hover, F. S., Miller, S. N. & Triantafyllou, M. S. 1997 Vortex-induced vibration of marine cables: Experiments using force feedback. *J. Fluids Struct*. **11**, 307–326.

Hover, F. S., Techet, A. H. & Triantafyllou, M. S. 1998 Forces on oscillating uniform and tapered cylinders in crossflow. *J. Fluid Mech.* **363**, 97–114.

Jauvtis, N. & Williamson, C. H. K. 2003 Vortex induced vibration of a cylinder with two degrees of freedom. *J. Fluids Struct*. **17**, 1035–42.

Khalak, A. & Williamson, C. H. K. 1996 Dynamics of a hydroelastic cylinder with very low mass and damping. *J. Fluids Struct*. **10**, 455–472.

Khalak, A. & Williamson, C. H. K. 1997 Investigation of the relative effects of mass and damping in vortex-induced vibration of a circular cylinder. *J. Wind Engng Ind. Aerodyn.* **69-71**, 341–350.

Khalak, A. & Williamson, C. H. K. 1999 Motions, forces and mode transitions in vortex-induced vibrations at low mass-damping. *J. Fluids Struct.* **13**, 813–851.

Klamo, J. T., Leonard, A. & Roshko, A. 2004 On the maximum amplitude in vortex-induced vibrations. *Bull. Am. Phys. Soc.* **49**, No. 9, 36.

Klamo, J. T., Leonard, A. & Roshko, A. 2005 On the maximum amplitude for a freely vibrating cylinder in cross-flow. *J. Fluids Struct.* **21**, 429–434.

Lucor, D. 2004 Generalized polynomial chaos: applications to random oscillators and flow-structure interactions. PhD thesis, Division of Applied Mathematics, Brown University.

Moe, G. & Overvick, T. 1982 Current-induced motions of multiple risers. In *Proc. BOSS-82, Behaviour of Offshore Struct.* (ed. C Chryyostomides & J. J. Connor), pp. 618–39. Hemisphere.

Morison, J. R., O'Brien, M. P., Johnson, J. W. & Schaf, S. A. 1950 The force exerted by surface waves on piles. *Petrol. Trans.* **189**, 149–157.

Naudascher, E. & Rockwell, D. 1994 Flow-Induced Vibrations: An Engineering Guide. Balkema.

Newman, D. J. & Karniadakis, G. E. 1997 Simulations of flow past a freely vibrating cable. *J. Fluid Mech.* **344**, 95–136.

Norberg, C. 2003 Fluctuating lift on a circular cylinder: review and new measurements. *J. Fluids Struct.* **17**, 57–96.

Obasaju, E. D., Bearman, P. W. & Graham, J. M. R. 1988 A study of forces, circulation and vortex patterns around a circular cylinder in oscillating flow. *J. Fluid Mech.* **196**, 467–494.

Owen, J. C., Bearman, P. W. & Szewczyk, A. A. 2001 Passive control of VIV with drag reduction. *J. Fluids Struct.* **15**, 597–606.

Parkinson, G. 1989 Phenomena and modelling of flow-induced vibrations of bluff bodies. *Prog. Aerospace Sci.* **26**, 169–224.

Roshko, A. 1993 Perspectives on bluff body aerodynamics. *J. Wind Engng Ind. Aerodyn.* **49**, 79–100.

Sarpkaya, T. 1978 Fluid forces on oscillating cylinders. *ASCE J. Waterway Port Coast. Ocean Div.* **104**, 275–290.

Sarpkaya, T. 1979 Vortex-induced oscillations. *Trans. ASME: J. Appl. Mech.* **46**, 241–258.

Sarpkaya, T. 1995 Hydrodynamic damping, flow-induced oscillations, and biharmonic response. *ASME J. Offshore Mech. Arctic Engng* **117**, 232–238.

Scruton, C. 1965 On the wind-excited oscillations of towers, stacks and masts. In *Proc. Symp. Wind Effects Build. Struct. Paper* 16, pp. 798–836. London: HMSO.

Shiels, D., Leonard, A. & Roshko, A. 2001 Flow-induced vibration of a circular cylinder at limiting structural parameters. *J. Fluids Struct.* **15**, 3–21.

Singh, S. P. & Mittal, S. 2005 Vortex induced oscillations at low Reynolds numbers: hysteresis & vortex-shedding modes. *J. Fluids Struct.* **20**, 1085–1104.

Skop, R. A. 1974 On modelling vortex excited oscillations. *NRL Memo. Rep.* 2927.

Skop, R. A. & Balasubramanian, S. 1997 A new twist on an old model for vortex-excited vibrations. *J. Fluids Struct.* **11**, 395–412.

Skop, R. A. & Griffin, O. M. 1973 An heuristic model for determining flow-induced vibrations of offshore structures. In *5th Offshore Technology Conf. OTC Paper* 1843, Houston, TX.

Smogeli, O. N. 2002 Design and evaluation of a force-feedback control system for VIV experiments. MS thesis. Department of Ocean Engineering, Masachussetts Institute of Technology.

Smogeli, O. N., Hover, F. S. & Triantafyllou, M. S. 2003 Force-feedback control in VIV experiments. *Proc. 22nd Intl Conf. on Offshore Mechanics and Arctic Engineering (OMAE03), June 8–13, 2003, Cancun, Mexico, Paper* OMAE2003-37340.

Sumer, B. M. & Fredsøe, J. 1997 Hydrodynamics around Cylindrical Structures. World Scientific.

Triantafyllou, M. S., Hover, F. S. & Techet, A. H. 2004 The effect of Reynolds number on VIV: from subcritical to supercritical flow. *Proc. 8th Intl Conf. on Flow Induced Vibrations, FIV 2004, Paris, France, 6–9 July* (ed. E. de Langre. & F. Axisa), p. 303.

Vickery, B. J. 1990 Progress and problems in the prediction of the response of prototype structures to vortex-induced excitation. *J. Wind Engng Ind. Aerodyn.* **33**, 181–196.

Vickery, B. J. & Watkins, R. D. 1964 Flow-induced vibrations of cylindrical structures. In *Proc. 1st Aust. Conf. Hydraul. Fluid Mech.* (ed. R. Silvester), pp. 213–241. Pergamon.

Vikestad, K. 1998 Multi-frequency response of a cylinder subjected to vortex shedding and support motions. Dr.Ing. thesis. Department of Marine Structures, Norwegian University of Science and Technology.

Williamson, C. H. K. 1996 Vortex dynamics in the cylinder wake. *Annu. Rev. Fluid Mech.* **28**, 477–539.

Williamson, C. H. K. & Govardhan, R. 2004 Vortex-induced vibrations. *Annu. Rev. Fluid Mech.* **36**, 413–455.

Williamson, C. H. K. & Roshko, A. 1988 Vortex formation in the wake of an oscillating cylinder. *J. Fluids Struct.* **2**, 355–381.

Zdravkovich, M. M. 1990 On origins of hysteretic responses of a circular cylinder induced by vortex shedding. *Z. Flugwiss. Weltraumforsch.* **14**, 47–58.